Numerical Simulation of an Intense Squall Line during 10–11 June 1985 PRE-STORM. Part II: Rear Inflow, Surface Pressure Perturbations and Stratiform Precipitation

DA-LIN ZHANG* AND KUN GAO**

National Center for Atmospheric Research,† Boulder, Colorado

(Manuscript received 7 September 1988, in final form 6 April 1989)

ABSTRACT

An intense rear-inflow jet, surface pressure perturbations, and stratiform precipitation associated with a squall line during 10–11 June 1985 are examined using a three-dimensional mesoscale nested-grid model. It is found that the large-scale baroclinity provides favorable and deep rear-to-front flow within the upper half of the troposphere and the mesoscale response to convective forcing helps enhance the trailing extensive rear inflow. However, latent cooling and water loading are directly responsible for the generation of the descending portion of the rear inflow. The role of the rear inflow is generally to produce convergence ahead and divergence behind the system, and thus assist the rapid acceleration of the leading convection when the prestorm environment is convectively favorable and the rapid dissipation of the convection when encountering unfavorable conditions. In this case study, the rear-inflow jet appears to have caused the splitting of the surface wake low as well as the organized rainfall.

As considerable mass within the rear inflow subsides, an intense surface wake low is formed at the back edge of the squall system. This result confirms previous observations that the surface wake low develops hydrostatically as a consequence of adiabatic warming and drying by the descending rear inflow. The wake low is shown to be an end product of complicated reactions involving condensate production, fallout cooling and induced subsiding motion. It does not have any significant effects on the evolution of atmospheric features ahead but contributes to vertical destabilization over the wake region.

The simulation shows that the squall line initially leans downshear and later upshear as the low-level cold pool progressively builds up and the system moves into a convectively stable environment. During the mature stage, there are three distinct airflows associated with the squall system: a leading overturning updraft and an ascending front-to-rear (FTR) current that both are driven by high-θ_e air from the boundary layer ahead of the line, and an overturning downdraft carrying low-θ_e air from the rear. These features resemble previously published results using nonhydrostatic cloud models. Due to continuous deposit of FTR momentum at the upper levels, the FTR updraft is responsible for the rearward transport of high-θ_e air mass for the generation of the trailing stratiform precipitation.

Several sensitivity experiments are conducted. The generation of the descending rear inflow, and the surface and midlevel pressure perturbations are found to be most sensitive to the parameterized moist downdrafts, hydrostatic water loading, evaporative cooling and ice microphysics, in that order. Without any one of these model processes, neither the rear inflow reaches the surface nor the surface mesohigh and wake low become well developed. The results illustrate that the descending rear inflow is a product of the dynamic response to the latent-cooling-induced circulation. Different roles of the parameterized versus grid-resolved downdrafts in the development of the descending rear inflow are also discussed.

1. Introduction

Squall lines with trailing stratiform precipitation frequently exhibit an enhanced region of midlevel relative flow extending into the interior of the storm from the rear (Smull and Houze 1987b). The magnitude of this type of rear inflow usually ranges from a couple of meters per second to over 15 m s^{-1}. In some cases, rear inflow was observed to extend downward and forward to near the leading edge of the surface outflow (e.g., Chong et al. 1987). As air in the unsaturated rear inflow continuously descends beneath the stratiform region, the resultant subsidence warming sometimes leads to the development of mesoβ-scale surface wake lows at the back edge of stratiform rainfall (Johnson and Hamilton 1988; Menard et al. 1988). Although rear inflow has been qualitatively described as one of the squall-line circulation features for more than four decades (Hamilton and Archbold 1945; Newton 1950), its actual importance on the evolution of the system and the mechanisms whereby it forms have never been a primary research concern. However, recent obser-

* Present affiliation: Department of Physics, University of Toronto, Toronto, Ontario, Canada.

** On leave from Department of Geography, Hang-zhou University, People's Republic of China.

† The National Center for Atmospheric Research is funded by the National Science Foundation.

Corresponding author address: Dr. Da-Lin Zhang, Department of Physics, University of Toronto, Toronto, Ontario, Canada, M5S 1A7.

vational studies by Augustine and Zipser (1987) and Smull and Houze (1985; 1987b) using high-resolution datasets document the pronounced rear-inflow jets descending toward the leading convective line through the stratiform region. In particular, a comprehensive literature survey of rear inflow cases by Smull and Houze (1987b) has revived much interest in the investigation of the governing dynamics and relationships among rear inflow, surface pressure perturbations, and stratiform precipitation.

The formation of rear inflow has been attributed by Smull and Houze (1987b) to the dynamic response to mesoscale convective systems (MCSs) rather than to a current of air from the large-scale environment overtaking the MCSs. However, it is not well established whether or not rear inflow would in turn affect the evolution of MCSs, nor has a comprehensive mechanism been demonstrated. A mass budget estimation by Chong et al. (1987) indicates that mesoscale downdrafts within the trailing stratiform region, which account for roughly 60% of a deep rear inflow, play an important part in the generation of convective updrafts along the leading gust front. On the other hand, Smull and Houze (1985; 1987b) argued that the forward penetration of rear-inflow jets into the convective leading edge may be responsible for the forward acceleration and subsequent rapid decay of deep convection along the squall-system's leading line. Menard et al. (1988) found that the formation of a wake low, which resulted from a descending rear-inflow jet during the mature stage, tends to dynamically destabilize the MCS wake region through enhanced convergence, eventually leading to the development of new intense convection. Johnson and Hamilton (1988) and Rutledge et al. (1988) also observed the development of weak convective cells some distance to the rear of a squall line as a consequence of such mass and moisture convergence.

Several hypotheses for the generation of rear inflow have been proposed, but neither the mechanisms whereby rear inflow forms nor the governing dynamics are well understood due to limited observational data and insufficient theoretical insight. Smull and Houze (1987b) proposed that the following two separate processes may be responsible for the generation of rear inflow: (i) hydrostatic reduction of pressures under rearward-sloped warm convective updrafts (LeMone 1983; LeMone et al. 1984); and (ii) the development of midlevel mesolows in the trailing stratiform region in association with latent heating above lower-level melting and evaporative cooling (Brown 1979). Midlevel air in the rear of the storm would then be expected to accelerate towards the low pressure center in the interior of MCSs. Lafore and Moncrieff (1989) also found in two-dimensional squall line simulations that horizontal pressure and temperature gradients, which result from latent heat release in the convective region and mesoscale unsaturated descent to the rear of the squall line, can lead to the development of rear inflow. Experimental cloud simulations by Weisman et al. (1988) show that strong and deep wind shear conditions are favorable for the generation of rear inflow and that this development is forced by the cold pool circulation which draws air into the descending branch of the convective zone.

Using the high-resolution PRE-STORM (Preliminary Regional Experiment for STORM–Central, see Cunning 1986) network dataset, Augustine and Zipser (1987), Smull and Houze (1987b), Johnson and Hamilton (1988) and Rutledge et al. (1988) analyzed the development of descending rear inflow in association with surface pressure perturbations, stratiform precipitation and other mesoβ-scale features in an intense squall line during 10–11 June 1985. In addition, Zhang, Gao, and Parsons (1989) (hereafter referred to as ZGP) showed in Part I of this series of papers that the PSU/NCAR (the Pennsylvania State University/National Center for Atmospheric Research) three-dimensional mesoscale model simulated remarkably well many of these observed mesoβ-scale structures and evolution from conventional meteorological observations. Specifically, the model reproduced the initiation of the squall line at nearly the right time and location; the generation of a pre-squall mesolow, a squall-induced mesohigh and a wake low; the vertical relative flow configuration of front-to-rear (FTR) motion at both upper and lower levels with an intermediate rear-to-front (RTF) flow jet; the maintenance and intensification of a mesovortex; and the leading convective rainfall followed by a transition zone and trailing stratiform precipitation (see ZGP for more details). Therefore, confidence in the simulation has been established by ZGP so that the model is sufficiently physically realistic for utilization in a more comprehensive study of the 10–11 June squall events.

The purpose of this study is to use the nested-grid model simulation described by ZGP to examine the detailed structure and evolution of the rear-inflow jet, its relationship to the surface pressure perturbations, stratiform rainfall and the leading squall line. In particular, the simulation provided dynamically consistent four-dimensional, high-resolution information with which the previously mentioned mesoscale features can be examined in much greater detail than is possible even with the network dataset. Another objective of this study is to use the model as a tool to explore the mechanisms important in the development of the 10–11 June rear inflow jet, wake lows and stratiform precipitation. In section 2, the vertical structure and evolution of the normal-line relative flow, and its relationship to the convective forcing and surface pressure distribution are shown. Section 3 presents three-dimensional flow structure and air trajectories associated with the squall system. Section 4 describes the effects of latent cooling and water loading on the generation of the descending rear-inflow jet, the surface mesohigh

and wake low. Section 5 discusses scales of atmospheric motion involved in the development of the rear-inflow jet and the effects of the squall line on the large-scale environment. A summary and concluding remarks are given in section 6.

2. Mesoβ-scale structure and evolution

The nested-grid model was initialized at 1200 UTC 10 June 1985 and integrated for 24 h with a fine-mesh length of 25 km (see ZGP for more details). One should note that the use of this grid size tends to produce aliasing of certain convective features, particularly for those along the leading line. The model simulation shows that the 10–11 June squall line was initiated when a southeasterly propagating weak surface front encountered a convectively unstable thermal boundary over the western Kansas–Oklahoma area around 2100 UTC 10 June (i.e., 9 h into simulation). The squall line rapidly dissipated after 0500 UTC 11 June as the system entered a convectively unfavorable environment. Before discussing the generation and subsequent evolution of the rear-inflow jet and the associated circulation characteristics, let us first inspect the hourly evolution of the simulated sea-level pressure distribution after the initiation of the squall line in a subdomain framework (see Fig. 1 in ZGP for the nested-grid domain). The related features prior to the onset of the squall line have been detailed in ZGP. From Figs. 6 and 9 in ZGP and Fig. 1 herein, the model overgenerated a convective system to the southwest of the squall line during the first few model hours; an associated mesohigh was entering northwestern Texas between 2200 and 0000 UTC. This feature quickly decayed after 0000 UTC, however, and did not appear to have any significant effect on the subsequent evolution of the squall events.

Following the initiation of the squall line, convective forcing gradually overwhelmed the frontal forcing in controlling the surface pressure distribution as well as other surface fields (see ZGP). Hence, a circularly shaped mesolow, which was initially located ahead of the surface front, progressively evolved into an elongated mesolow in advance of the squall line (i.e., pre-squall mesolow, see Fig. 1). Around 2300 UTC, a squall-induced mesohigh was generated behind the leading convective line. This mesohigh could be attributed to the parameterized moist downdrafts in the Fritsch–Chappell (1980) convective scheme and resolvable-scale evaporative cooling, melting and water loading. Near 0000 UTC, a surface wake low emerged to the rear of the squall system and reached its maximum intensity at 0600 UTC. The pre-squall mesolow, squall-induced mesohigh and wake low are best defined in the simulation at 0500 UTC. Subsequently, the mesohigh and the squall line dissipated rapidly. An area-averaged peak resolvable-scale updraft also indicates a rapid decrease in magnitude thereafter (Fig. 2). It is interesting that the surface wake low began to split into two parts after 0400 UTC: one gradually propagated eastward out of the network and the other became well developed over central Oklahoma at 0900 UTC. Johnson and Hamilton (1988) also documented the splitting of the wake low during this stage. It is evident from Figs. 1 and 2 that the evolution of the model squall line can be roughly divided into three stages: an incipient stage before 0100 UTC; a mature stage between 0100 and 0500 UTC; and a dissipation stage after 0500 UTC. Thus, the following discussion is organized according to the lifecycle of the squall system.

a. Incipient stage

Figure 3 shows the vertical cross sections of simulated horizontal relative flow, vertical motion, height deviations and relative circulation vectors over the same period as for Fig. 1. The relative flow was computed by subtracting the squall line's propagation velocity of 14.5 m s^{-1} towards the direction of 125° (i.e., southeastward). The associated circulation flow vectors were plotted only in a relative sense for individual cross sections. All (height and temperature) deviations were obtained by deducting their pressure-level averages in the cross section. For convenience in later discussion, Fig. 4 shows two-hourly cross-sectional analyses of equivalent potential temperatures (θ_e), temperature deviations, divergence and potential temperatures (θ). All cross sections lie within a fixed vertical plane (with different segments used to follow the system) in which the continuous history of the rear-inflow jet was found to be best portrayed; each cross section covers an identical horizontal extent of 475 km. This cross-sectional plane is placed to be as perpendicular as possible to the squall line, particularly during the mature and decaying stages.

At 2200 UTC, the distribution of relative flow featured a deep layer of a FTR current with its maximum occurring near the surface, a 250 mb layer of a RTF current above 500 mb that extended forward and upward until it reached the tropopause ahead of the leading line, and an upper-level rearward current behind the leading line. There was a strong wind shear at the lowest levels ahead of the squall line (Fig. 3a). Similar magnitude of the low-level wind shear was used by Thorpe, Miller and Moncrieff (1982, hereafter TMM) and Rotunno, Klemp and Weisman (1988, hereafter RKW) and Weisman et al. (1988), for theoretical studies of long-lived squall lines. They found that such a low-level wind shear is favorable for the generation of deep and vigorous convection when interacting with an extensive cold pool. Since this is the time when the simulated squall line was initiated for just one to two hours, the basic flow structure more or less represented the mesoscale wind distribution in the vicinity of the MCS during its incipient stage, except for upper levels which were dominated by outflow from the squall line.

During this incipient stage, the simulated squall line

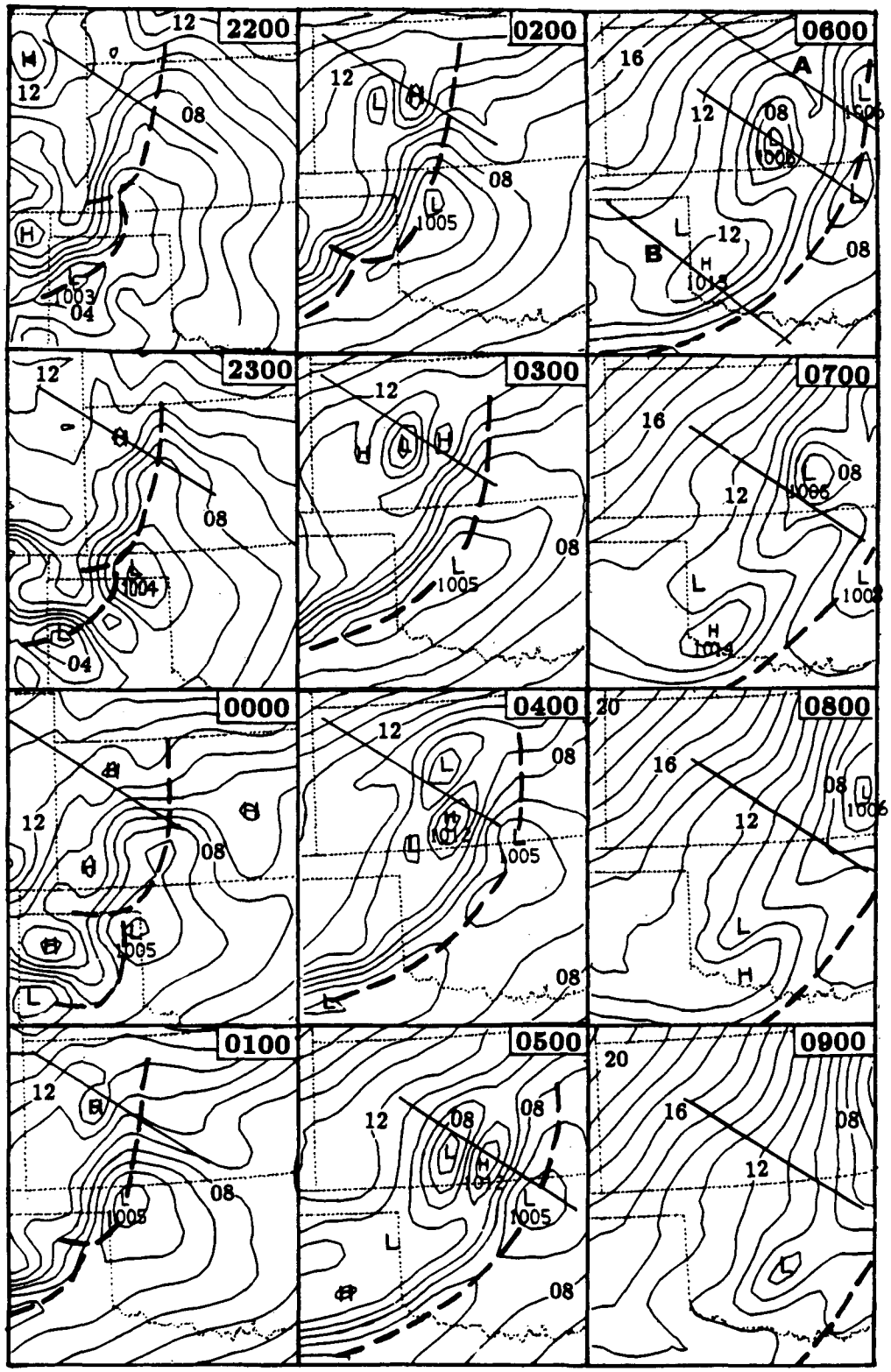

FIG. 1. Distribution of sea level pressure (mb) at intervals of 1 mb from 10 to 21 h simulations, verified for the period between 2200 UTC 10 and 0900 UTC 11 June 1985. Thick dashed lines denote the advancing cold outflow associated with the squall line. Thick solid lines are the cross sections used for the subsequent figures, and letters "A" and "B" in 0600 frame denote cross sections used in Figs. 5 and 6, respectively.

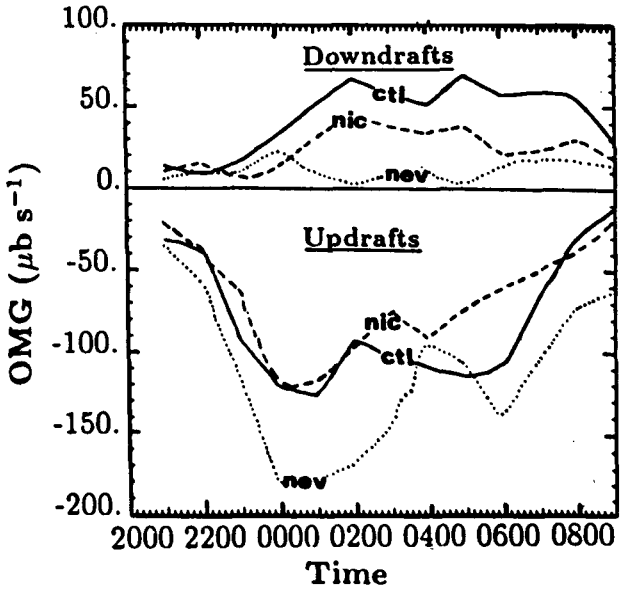

FIG. 2. The predicted hourly 9-point-averaged maximum mesoscale updrafts ($\omega \leq 0$) and downdrafts ($\omega \geq 0$) for simulations of the control (CTL), no ice (NIC) and no evaporation (NEV).

was characterized by an organized mesoscale ascent and a major portion of the updraft leaned downshear (Fig. 4). Significant water was precipitated from the updraft on the downshear side; the resulting latent cooling appears to cause the subsequent enhancement of sinking motion ahead of the line (see 2300 UTC frame). A branch of high-θ_e air at the lowest levels flowed through the rainfall region and then descended to the rear. This descent was associated with the cooling from both resolvable-scale and parameterized convection. These results are very interesting since they are qualitatively similar to that produced by nonhydrostatic cloud models with much smaller grid sizes, such as TMM and RKW. Since these structures were hydrostatically produced in this model, they should be related to convectively generated mass perturbations, namely, the height deviations. Specifically, because the height deviation is closely related to the vertical integration of the buoyancy field, the presence of positive deviations (e.g., a warm-core-related mesohigh at the top of the updraft) tends to produce mass convergence underneath and divergence aloft by buoyancy and outward acceleration by horizontal pressure gradient forces (cf. Figs. 3a and 4). The opposite is true for the presence of negative deviations (e.g., a midlevel mesolow). As Figs. 3a–c and 4 show, these mesohighs (lows) of height deviations were located above levels where the layer-integrated warming (cooling) was maximized, and persisted during almost the whole lifetime. Because the squall line propagated southeastward along with a traveling mesoα-scale trough–ridge system (see Figs. 3 and 14 in ZGP), there was a systematic RTF height (temperature) gradient in the background of the mid-to-upper troposphere (cf. Figs. 3a–c and 4). Although the above-mentioned mesoβ-scale pressure perturbations tended to determine the structure and evolution of the squall line, the general background height distribution clearly provided a favorable condition for the subsequent development of the FTR flow and trailing stratiform precipitation. At the low levels, the presence of the surface front resulted in a FTR height (temperature) gradient which continued providing the necessary forcing for the initiation of deep convection along the leading line.

One hour later (i.e., 2300 UTC), the leading updraft intensified considerably in response to the rapid latent heat release. As a consequence, substantial upward momentum transport broke through the mid-to-upper level RTF flow channel into the upper-level outflow and deep rear inflow was immediately formed behind the system (Fig. 3a). As will be shown in a forthcoming article on a momentum budget study, the convectively generated mesohigh near the tropopause has a significant contribution to the enhancement of the upper-level outflow, and the continuous momentum generation and transports were responsible for the rapid deposit of the rearward momentum aloft (LeMone 1983; LeMone et al. 1984) and for the subsequent development of extensive stratiform precipitation. Specifically, when the squall line propagated faster than its environmental winds, it tends to leave in its wake a series of decaying cloud towers and anvils. This is particularly true in the present case for upper levels where detrainment from deep convection plus the convectively enhanced FTR outflow could efficiently generate a near-saturated stratiform region to the rear of the system. Moreover, the momentum transport and generation during the past one hour altered the flow regime from the predominantly "overturning updraft" type (Moncrieff 1978; 1981) to the coexistent structure of the "FTR and overturning updrafts" (see TMM).

By 0000 UTC (i.e., 12 h into simulation), the leading portion of the rear inflow began to lower (Fig. 3a). Associated with the lowering was the development of sinking motion within the rear inflow. Figures 3a and 4 depict that this lowering coincides with the development of a mesohigh (or cold pool) near the surface. Notice that this mesohigh gradually separated from the leading surface front as it moved southeastward. In addition, air parcels on the downshear side of the updraft became more negatively buoyant after being displaced upward, and then descended to the rear, thereby further enhancing the surface cool pool (mesohigh). Thus, the mesoscale downdraft tilted downshear and commenced at the levels where the FTR low-θ_e air inflow was the strongest. As a result, the original updraft was undercut at that level and a new updraft was triggered near the line. Similar behavior is evident in Figs. 11b and 11c of RKW.

By 0100 UTC (i.e., four hours after the initiation of the squall line), the rear-inflow jet has significantly

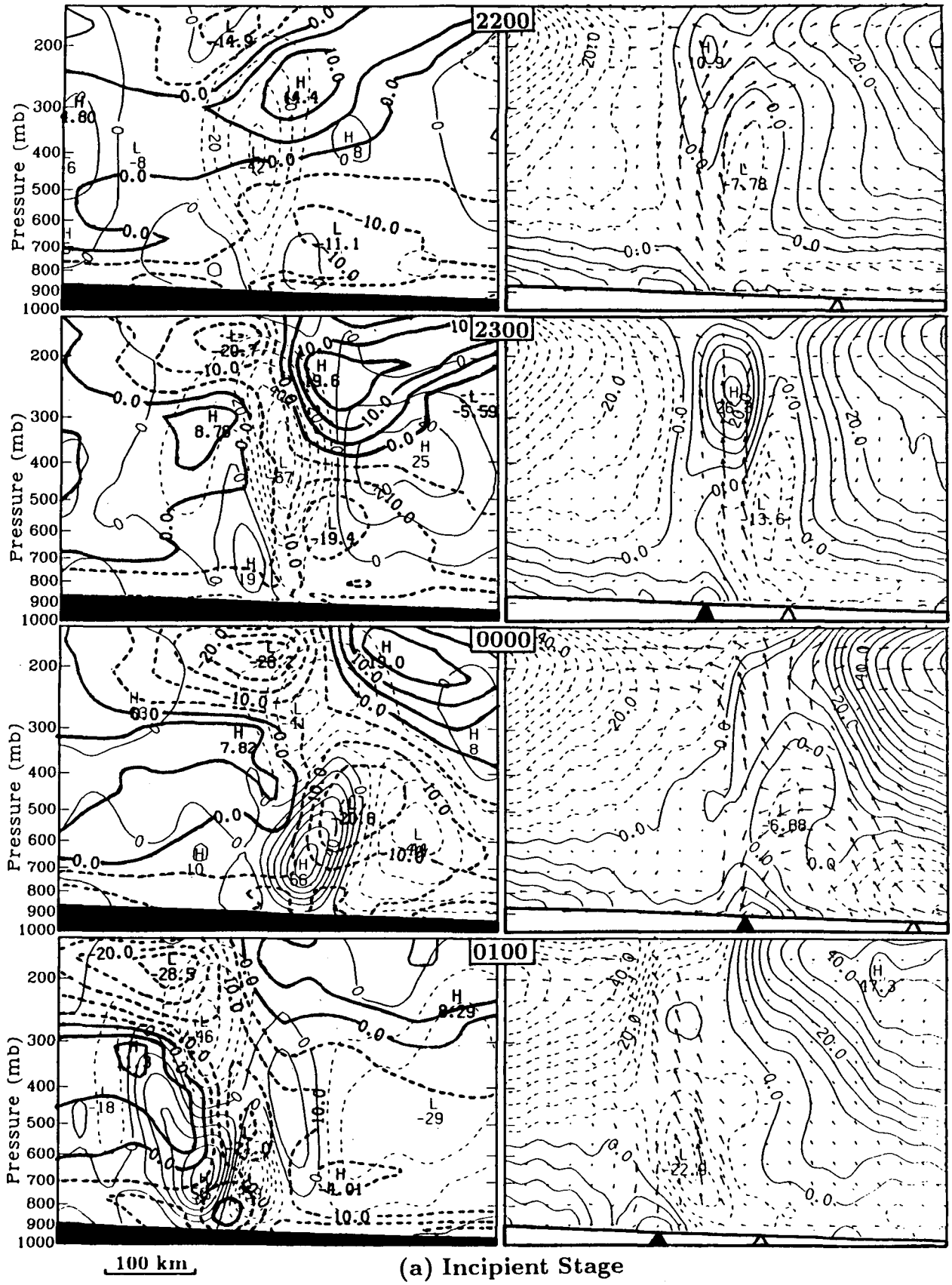

FIG. 3. Left panel shows the hourly evolution of NW–SE vertical cross-sectional distribution of relative normal-line flow at intervals of 5 m s^{-1} [thick solid (dashed) lines denote RTF (FTR) flow], and vertical motion (ω, μb s^{-1}) at intervals of 10 μb s^{-1} [thin solid (dashed) lines indicate downward (upward) motion] from 10 to 21 h simulations,

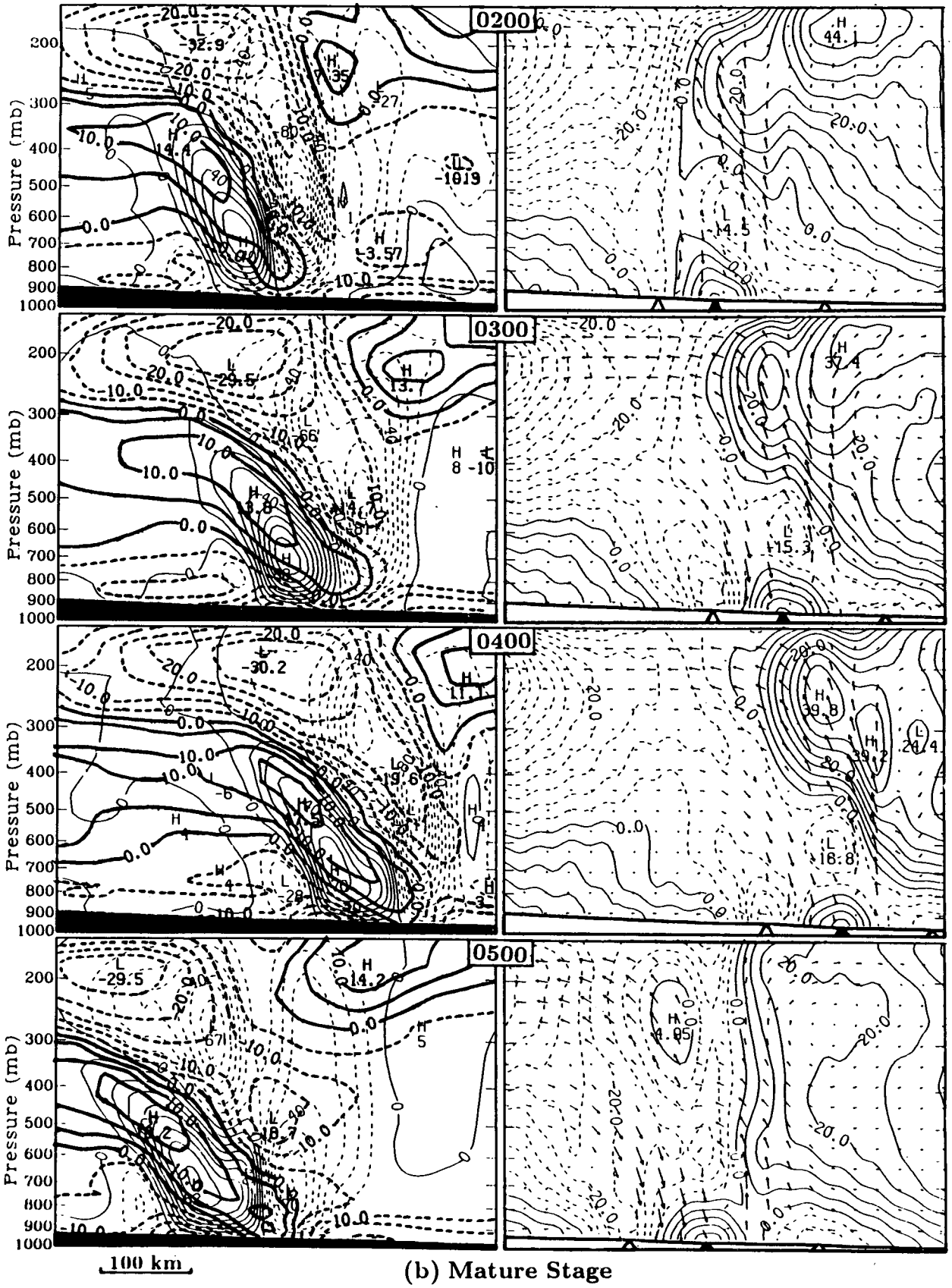

FIG. 3 (*Continued*) verified for the period between 2200 UTC 10 and 0900 UTC 11 June 1985. Right panel shows the corresponding distribution of relative circulation vectors (normal to the line) and height deviations [m, solid (dashed) lines indicate positive (negative) values] at intervals of 5 m.

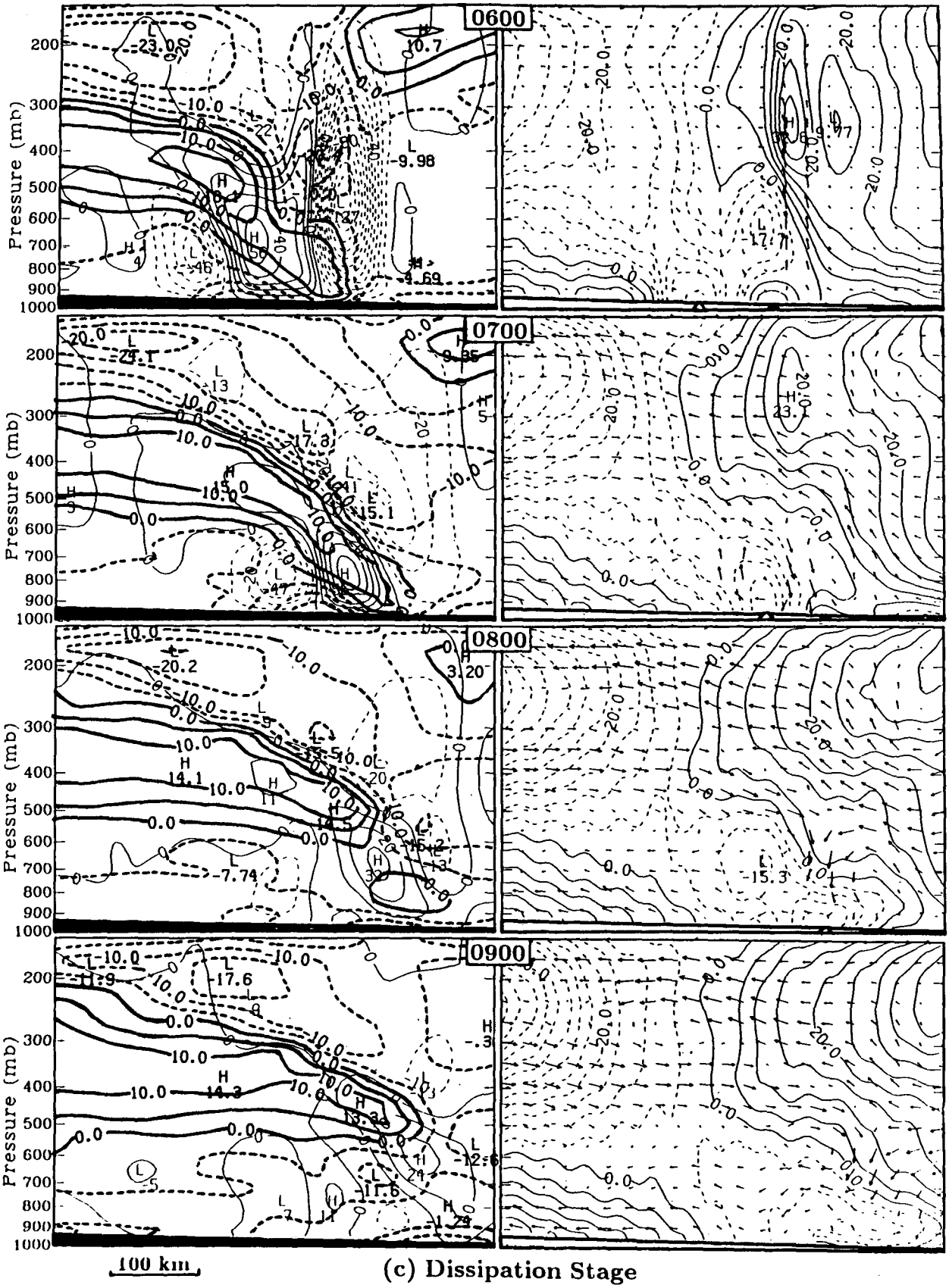

FIG. 3 (*Continued*) Solid (open) triangles indicate the position of surface mesohighs (mesolows). Cross sections at individual times are taken along lines as given in Fig. 1 and cover a horizontal size of 475 km.

lowered from above 500 mb to near 650 mb in two hours. Of particular interest is the development of a very weak RTF flow between the organized updraft and downdraft at the lowest levels. Since this feature was situated ahead of the intensifying surface mesohigh (cf. Figs. 1 and 3a), it must be associated with cold outflow in which air parcels were accelerated forward by the resulting strong pressure gradient. As the rear inflow descended forward towards the leading convective line, the mesoscale downdraft began to tilt upshear and commenced at the top of the slanted rear-inflow jet with its orientation coincident with the descending portion of the rear inflow. Due to the upshear tilt, another alteration in the circulation pattern ensued. That is, the vertical circulation now consists of three distinct currents: an overturning updraft near the leading line, a FTR penetrative updraft and an overturning downdraft to the rear of the system. This airflow structure resembles an idealized cloud model of airflow as produced by nonhydrostatic cloud models, such as TMM, RKW, Weisman et al. (1988) and Lafore and Moncrieff (1989).

Note that a well-defined midlevel mesolow developed ahead of the descending rear-inflow jet. This mesolow is hydrostatically generated by continued latent heating above melting and evaporative cooling (Brown 1979), and thus sandwiched between the surface and upper-level mesohighs. The surface mesohigh lacks slightly behind the midlevel mesolow due to the latent heating occurring in advance of the latent cooling. We feel that the development of the midlevel mesolow is crucial in determining the internal circulation pattern of the squall line. Specifically, the boundary-layer high-θ_e air ahead of the line tends to be accelerated rearward by the mesolow while being forced upward by buoyancy. At the same time, the mesolow tends to accelerate the midlevel low-θ_e air to the rear of the system forward as it descends in the downdrafts.

b. *Mature stage*

Five hours after the initiation of the squall line (i.e., 0200 UTC), nearly all squall properties became well developed although they still kept intensifying (Fig. 3b). In particular, the descending rear inflow has considerably strengthened as the low-level mesohigh generated RTF outflow was overtaken by the subsiding air within the rear inflow. The rear inflow stretched well *ahead of the surface mesohigh* and into the leading updraft. Some low-θ_e air within the rear inflow was entering the updraft and affecting the intensity and evolution of the leading convective activity. Chong et al. (1987) also found such a phenomenon in an African squall line. Furthermore, we noticed that the rear inflow jet in the present case was distributed over a 450 km distance along and behind the line, as will be seen in the next section, but stronger rear inflow occurred at a location where an intense mesohigh developed.

It is also evident from Figs. 3b and 4 that the intensification of the descending rear inflow was associated with the rapid build-up of the low-level cold pool (mesohigh). The maximum descending within the rear inflow exceeded 60 $\mu b\ s^{-1}$ (Fig. 2). Because the resulting subsidence warming gradually overwhelmed melting and evaporative cooling toward the rear, the cold pool diminished and then a well-defined net warming pocket emerged at the back edge of the squall system and to the place where the sinking persisted the longest (cf. Fig. 3b and 0400 UTC frame in Fig. 4). As a result, a surface wake low was hydrostatically generated below (Fig. 1) with its trough axis tilted rearward in the low troposphere in a fashion similar to the descending portion of the rear inflow (Fig. 3b). From a dynamic viewpoint, it is apparent that the distribution of the wake low and the midlevel mesolow determines the breadth and slope of the descending flow regime. Since the descending rear inflow was primarily driven by the latent cooling, *the wake low can be regarded as an end product of a chain of complicated dynamic reactions from convectively generated condensate to water loading, latent cooling, the surface mesohigh and from the generation of the midlevel mesolow to the enhanced descending rear inflow and adiabatic warming and drying*. The generation of the surface wake low by subsidence warming from the descending rear inflow confirms the Johnson and Hamilton (1988) observations showing that the wake low is a surface manifestation of the rear-inflow jet. Although the upper-level trailing stratiform region also exhibited widespread warming and moistening, as shown by decreases in the vertical θ and θ_e gradients between 250 and 200 mb (Fig. 4), it evidently contributed little to the development of the surface wake low.

Note the distribution of θ and θ_e that shows the buildup of a low-level cold pool, a midlevel warm core, an upper-level cold dome and the lifting of the tropopause (Fig. 4). The response of the horizontal wind field to this vertical thermal structure led to low-level divergence, midlevel convergence and upper-level divergence. The maximum convergence occurred at the level where the updrafts and downdrafts were originating, suggesting that the midlevel mass convergence fed both the updrafts and downdrafts (Houze 1977). Note also two opposite currents (i.e., the FTR and RTF) that interfaced within a deep layer up to 300 mb. This resulted in large mass convergence along the interface between these two currents ($\leqslant 4 \times 10^{-4}\ s^{-1}$). Such large convergence clearly helped trigger new convection along the leading line during this period. Of further interest is that the tilted θ_e contour of 336 K corresponded well to the interface and acted as a material surface in separating the updrafts and downdrafts. This suggests that air parcels moving along the slantwise interface conserved their θ_e properties. In this context, ZGP showed (see their Fig. 22b) that the interface limited the downward extension (upward penetration) of

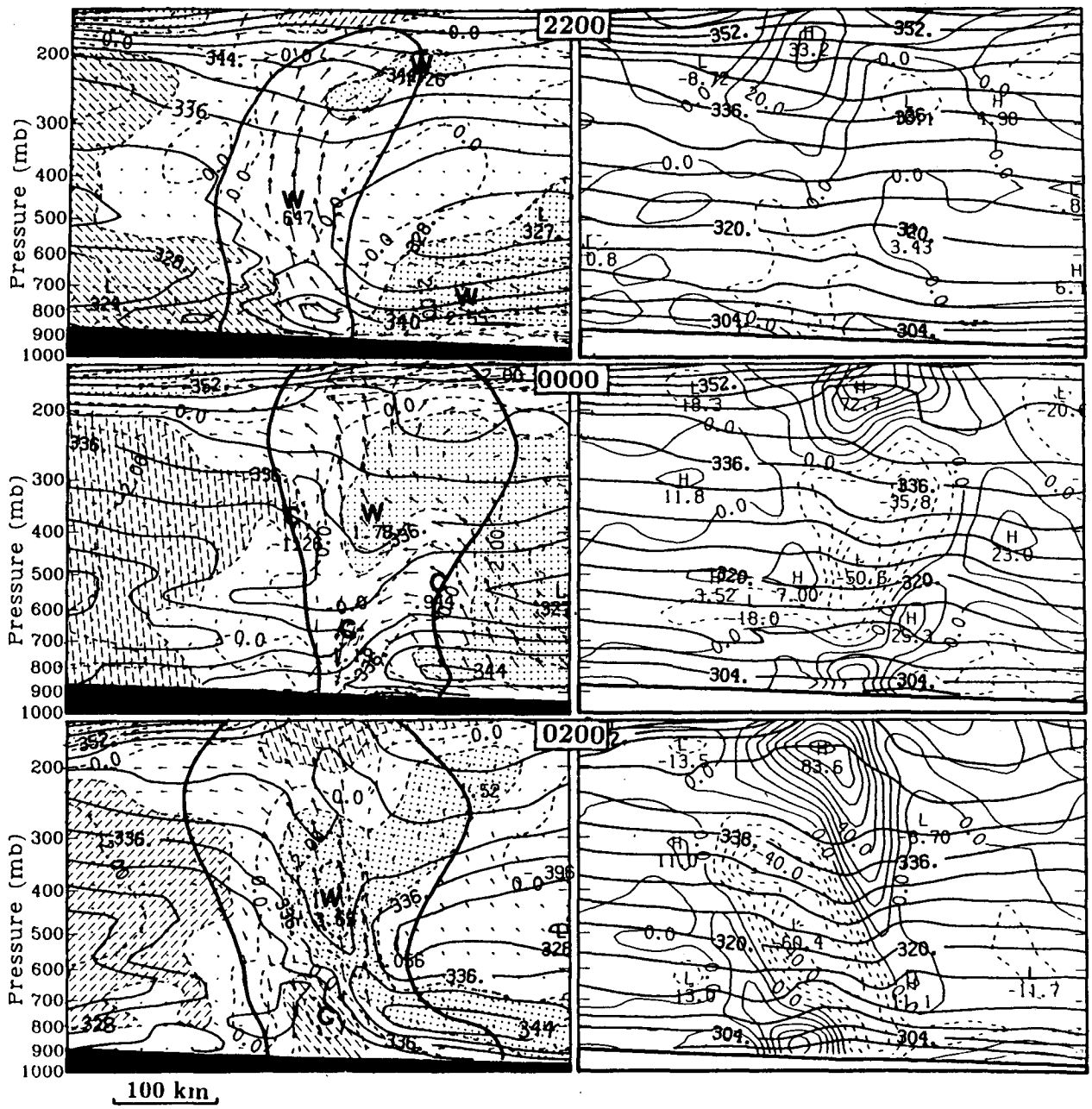

FIG. 4. Left panel shows the two-hourly evolution of NW–SE vertical cross sectional distribution of equivalent potential temperature (solid lines) at intervals of 4 K and temperature deviations (dashed lines) at intervals of 1°C superposed with relative circulation vectors (normal to the line) from 10 to 20 h simulation, verified at the times as indicated. Dotted shading shows temperature deviations larger than 1°C whereas dash-hatched shading shows temperature deviations less than −1°C.

the trailing stratiform rain (the wake-low generated convective activity) owing to the intense descending inflow of dry air into the system. This finding conforms to observational studies by Smull and Houze (1985), Rutledge et al. (1988) and Johnson and Hamilton (1988) that strong rear inflow often produces a notch or bowlike precipitation-free echo structure at the back edge of the stratiform rainfall. The θ_e distribution also clearly reveals that *the squall line was basically driven by boundary-layer high-θ_e air in the updrafts ahead of the system and gravitational sinking of midlevel low-θ_e air to the rear*. The oscillatory θ_e profile below 600 mb was found to be due to a steplike cooling by ice melting.

It is of particular interest that in association with the slanted θ_e and convergence distribution, the entire

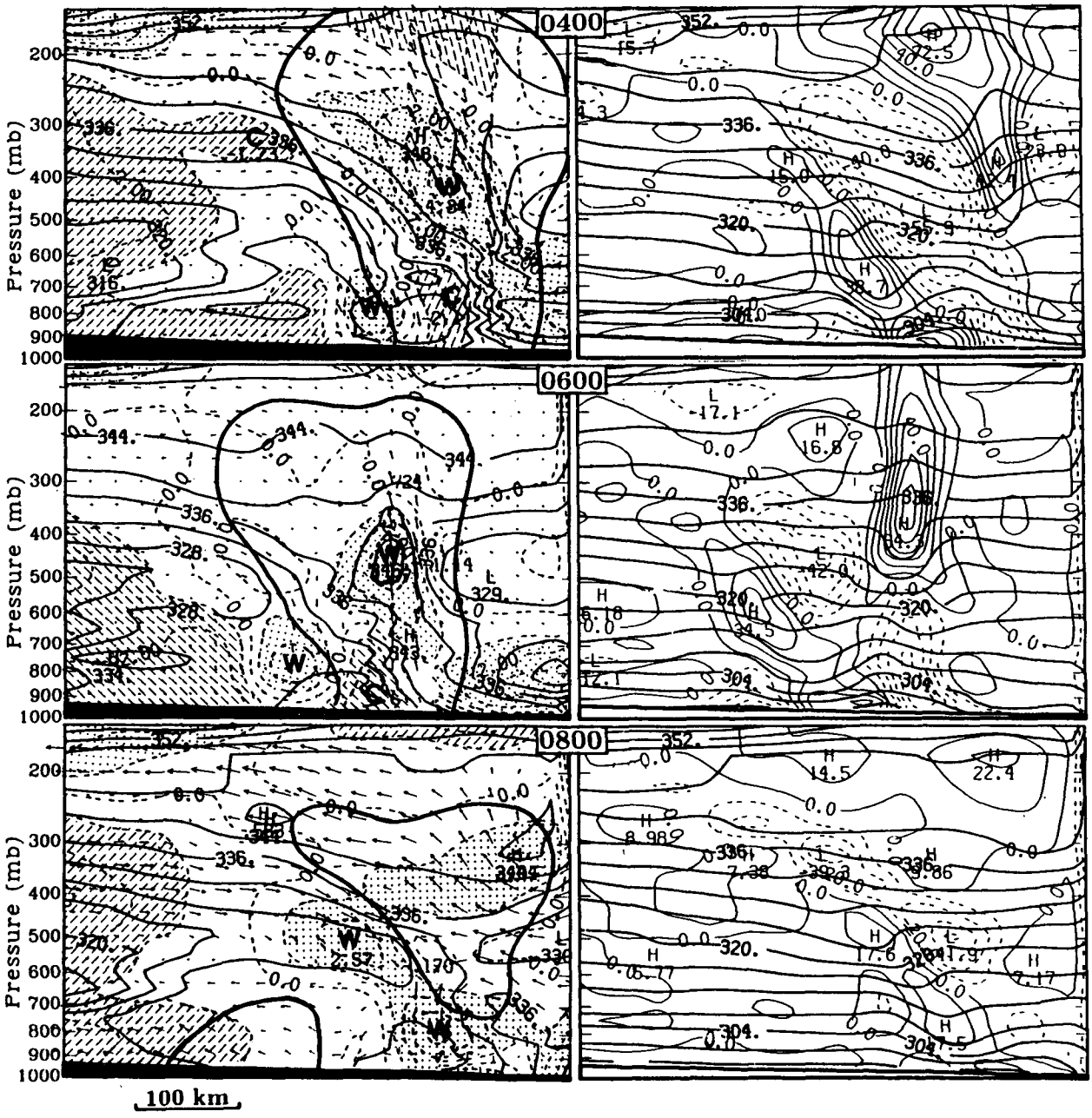

FIG. 4. (*Continued*) Letters "W" and "C" denote the local maximum and minimum temperature deviations, respectively. Thick solid line denotes rainwater content larger than 0.2 g kg^{-1}. Right panel shows the corresponding distribution of potential temperature (thick solid lines) at intervals of 4 K and divergence/convergence (thin solid/dashed lines) at intervals of 10^{-4} s^{-1}. Cross sections at individual times are taken along lines as given in Fig. 1 and cover a horizontal size of 475 km.

squall system gradually leans upshear during the two to three hour mature phase. This behavior is again similar to that produced by nonhydrostatic cloud models (TMM and RKW). It follows that the upshear and downshear tilts of updrafts (downdrafts) as well as the previously mentioned airflow patterns are not the inherent features of nonhydrostatic primitive equation models. Rather, they are determined by interaction among cloud microphysics, dynamic response to convective forcing, preexisting environmental flow and thermodynamic conditions. In particular, according to the RKW theory, the progressively upshear tilt in the present case could be well explained by the relationship between the low-level wind shear and the convectively generated cold pool (see schematic diagram 18 in RKW). Specifically, during the period of the squall development, the cold pool was relatively shallow and weak. Positive alongline horizontal vor-

ticity from the low-level strong wind shear was continuously transported into midto-upper levels in the updrafts. Thus, the system leaned downshear with dominant overturning type of airflow. As the convectively generated cold pool became deeper and stronger, the resultant negative alongline vorticity gradually overpowered the positive vorticity associated with the low-level wind shear. This caused the leading edge to tilt more and more upshear. In a theoretical study, Moncrieff (1978) showed in an initial-value problem that when a heat source was introduced in a shear flow, the flow response was to produce a downshear-tilted system. However, when a heat source located above a heat sink existed, the system became highly transient and the flow had an upshear orientation. In addition, we feel that continued deposit of upper-level rearward momentum may have also contributed to the upshear tilt. In particular, the rearward speed has been considerably intensified since the initiation of the line, namely, from -14.3 m s^{-1} at 2200 UTC (Fig. 3a) to the present -33.0 m s^{-1} (Fig. 3b). When coupled with the midlevel rear inflow, this upper-level outflow became a part of the vertical circulation which clearly exhibits negative alongline vorticity. This argument used to be widely accepted as being the explanation of the upshear slope in supercell storms (Newton 1966). It should be pointed out that this argument does not contradict the RKW theory when the momentum transport could be regarded to be negligible, since under such a circumstance, the upper-level rearward momentum was considered being completely generated by the upper-level mesohigh. In another theoretical study, Seitter and Kuo (1983) argued that water loading can affect the alongline vorticity production and also contribute to the upshear tilt of the updraft.

Over the period 0300 and 0500 UTC, the rear-inflow jet strengthened further with the 5 m s^{-1} isotach extending close to the ground. The perturbation of isotachs at the lowest 100 mb layer reflects the presence of surface pressure perturbations. Because of the increase in the low-level RTF flow component, the northern segment of the squall system accelerated southeastward faster than its southern portion (Fig. 1). Smull and Houze (1985) also observed such an acceleration of the leading convection (which resulted in a bowlike echo structure) as rear inflow became well developed. This further indicates that the development of the rear-inflow jet helps enhance the low-level convergence to generate new convection ahead of the system when entering a *convectively favorable* environment (see Fig. 27 in ZGP), a conclusion also reached by Lafore and Moncrieff (1989). The surface mesohigh and associated cold outflow have made a significant contribution to such enhancement.

Another interesting feature evident during this period (Fig. 3b) is the split of the mesoscale updrafts into two centers with one propagating rearward in the slantwise FTR updraft. The upward motion within this rearwardly moving updraft was as strong as 1 m s^{-1}, close to what Rutledge et al. (1988) have derived from Doppler radar data. This updraft was believed to be essential for the generation of the trailing stratiform precipitation when considering that a large amount of moisture has been transported into this region by the FTR penetrative updraft. In fact, Fig. 4 shows that the layer of high-θ_e air within the stratiform region has thickened considerably. Between these two updraft centers was a weak upward motion zone (Fig. 3b), with a rainwater minimum underneath (not shown) which qualitatively corresponds to the transition zone as defined by Smull and Houze (1987a). These vertical motion structures resemble quite well those typically observed in other midlatitude (see Figs. 15–18 in Ogura and Liou 1980) and tropical (see Figs. 15 and 16 in Gamache and Houze 1982) squall lines.

The transition zone has been found to be a common feature associated with squall lines with trailing stratiform precipitation. However, its actual cause has never been well established. Fig. 3b shows that the development of the transition zone could be related to the rearward movement of the upper-level mesohigh in the FTR updraft (see the 0300–0500 UTC frames). Specifically, as the system leaned increasingly upshear, a large amount of buoyant air mass was intermittedly transported into the rear to form the trailing stratiform precipitation. Thus, air parcels were accelerated more toward the rear in the ascending FTR updraft (see 0500 UTC). Dynamically speaking, as the upper-level mesohigh propagated rearward and/or as a new mesohigh associated with the leading updraft developed, the resulting higher-level divergence tended to produce descending motion superposed on the flow between. This would then cause the relatively fast fallout and possibly subsequent evaporation of precipitable water in that vertical column, eventually leading to the presence of the rainwater minimum in the low-to-midlevel, i.e., the so-called transition zone. Note the rearward transport of mesohighs by the FTR updraft from the lower-level high-θ_e region ahead of the line, which clearly shows that the generation of trailing stratiform precipitation can be considered as the rearward transport of decaying convective cells by the slanted updraft when the squall system begins to lean upshear.

c. *Dissipation stage*

As shown in ZGP, the squall line rapidly dissipated as it advanced into a more convectively stable environment. In addition, Fig. 3c shows that the leading squall updraft exhibited significant deceleration immediately after 0600 UTC. However, the succeeding rear-inflow jet still maintained its eastward propagation with little change in speed. Therefore, the leading updraft was quickly elevated by the descending rear inflow. This indicates that the descending rear inflow

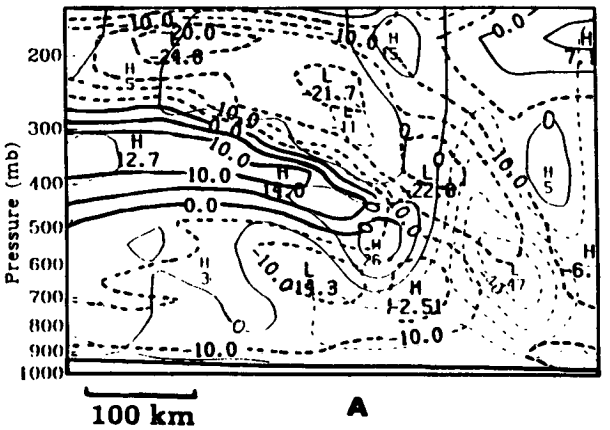

FIG. 5. Northwest–southeast cross section of relative flow (normal to the line) at intervals of 5 m s^{-1} [thick solid (dashed) lines denote RTF (FTR) flow], and vertical motion (ω, μb s^{-1}) at intervals of 10 μb s^{-1} [thin solid (dashed) lines indicate downward (upward) motion] from 18 h simulation verified at 0600 UTC 11 June. The cross section was taken along line A for 0600 UTC frame in Fig. 1 and covers a horizontal size of 475 km.

tends to suppress the occurrence of convective activity when encountering a *convectively unfavorable* environment. The sequence and processes of the dissipation could be briefly described as follows. First, the decline in high-θ_e air supply reduced the latent heating (see Fig. 27 in ZGP), and a disorganization of the updrafts ensued (Fig. 2). Meanwhile, the elevated leading updraft gradually lost its convective root in the boundary layer, allowing midlevel low-θ_e air to enter the system from both the front and rear, thus further weakening the intensity of the updraft (Fig. 3c). Then, the fallout of precipitable water rapidly depleted (see Fig. 33 in ZGP). Subsequently, the diminishing of water loading, melting and evaporative cooling led to the weakening of the surface mesohigh, the midlevel mesolow and the mesoscale downdraft, in that order. These processes ultimately caused the descending rear inflow to be detached from the low-level flow. Near the end of the simulation, the rear-inflow jet was totally elevated. It is interesting, however, that as the convective forcing (i.e., latent heating and cooling) weakened, little changes in the strength of the wake occurred (see 0600–0900 frames in Fig. 1). We observed that as the wake low moved out of the fine-mesh domain it became a gravity-wave type of perturbation which advanced relatively faster than the squall line and eventually merged with the presquall mesolow to the east of the network.

As mentioned in ZGP, the presence of a preexisting mesovortex assisted the organization of the rear-inflow jet, the surface mesohigh and wake low as an integral system. On the other hand, the intensification of the rear-inflow jet helped concentrate cyclonic vorticity associated with the vortex since the strongest rear inflow was found in the present case being located to the southwest of the vortex (see ZGP for more details). Actually, to the northeast of the vortex (see Fig. 1), Fig. 5 fails to show any sign of the rear inflow up to 500 mb owing to the compensating return (i.e., FTR) flow associated with the vortex circulation. Above 500 mb, the magnitude of the RTF inflow and the FTR outflow were similar to that to the southwest of the vortex.

Since both observations and the simulation showed the splitting of the wake low during this stage (Fig. 1), Fig. 6 displays a vertical cross section of relative flow and vertical motion through the southern mesolow at 0600 UTC. A much deeper but weaker rear inflow jet was associated with the more widespread and weak surface wake low at this time. The widespread nature was more likely associated with a surface mesohigh that just began to develop ahead of the wake low (Fig. 1). After the previous comprehensive discussions, we may now more easily understand why the wake low split during this period. ZGP showed that corresponding to the split of the wake low, both simulated convective and stratiform rainfall maxima also split into two centers between 0300 and 0600 UTC (see their Figs. 15 and 16) with the southern one coinciding with the surface mesohigh over southwestern Oklahoma. This splitting appears to occur at the place where stronger rear inflow was present. This argument is supported by observations by Johnson and Hamilton (1988) and Rutledge et al. (1988) that the precipitation-free echo at the back edge of the stratiform rainfall coincided with the location of the splitting. Thus, any or all of the following conditions may have contributed to the splitting of the rainfall maximum and the wake low: (i) more low-θ_e air from the rear-inflow jet entered the leading updraft; (ii) the leading updraft was lifted by the stronger rear-inflow jet as the system moved into the convectively unfavorable environment; and (iii) nonuniform larger-scale stratification may have been present ahead of the line.

Up to this point, we have showed evidence that the surface wake low can be indirectly related to the latent cooling and water loading. A question one may ask is:

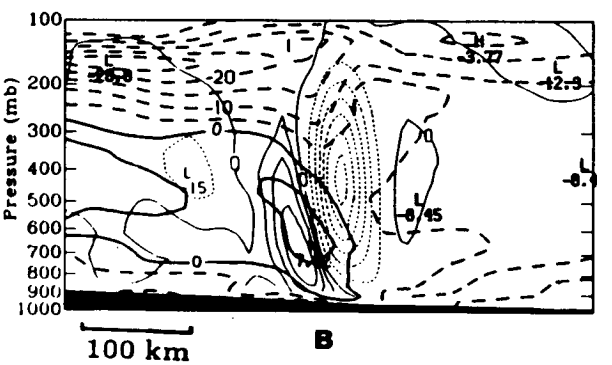

FIG. 6. As in Fig. 5 but for a cross section taken along line B in Fig. 1.

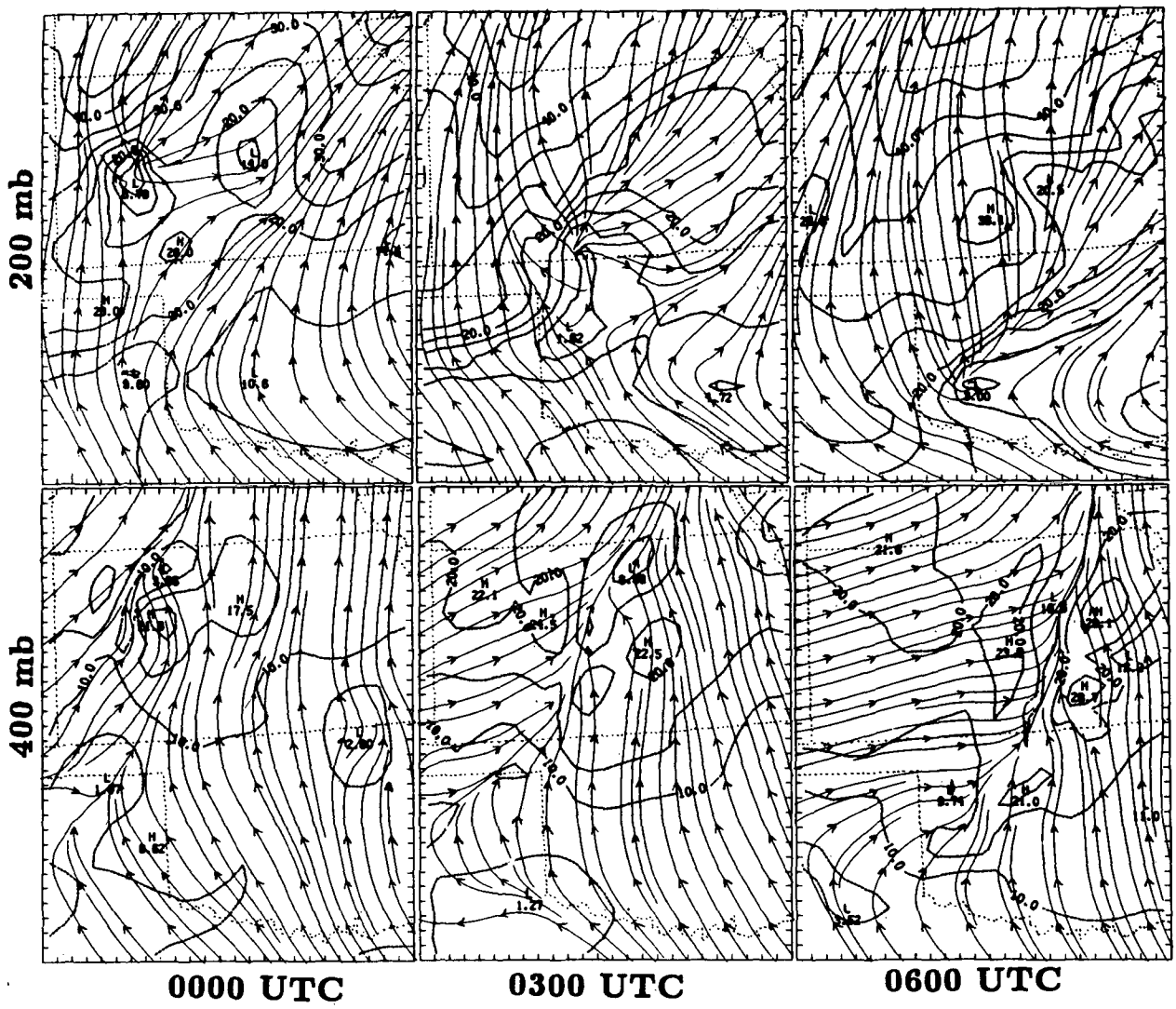

FIG. 7. Mesoscale relative flow streamline analysis from 12, 15 and 18 h simulations, verified at 0000, 0300 and 0600 UTC 11 June, respectively. Dashed lines denote isotachs at intervals of 5 m s^{-1}. Thick dashed lines on the surface chart are the position of cold outflow associated with the squall line.

does this wake low produce any significant feedback to the rear inflow, the leading convection or the trailing stratiform precipitation? The present simulation reveals that the wake lows appear to have moved passively with the system during the intensifying stage and lagged more than 150 km behind the leading line. It might be possible that the major wake low contributed to a surface mesocyclogenesis over the Iowa–Ohio Valley after merging with the pre-squall mesolow. Nevertheless, as previously mentioned, the wake low produced visible weather in the present case over the wake region. ZGP showed that the model generated well-developed surface convergence, favorable upward motion up to 600 mb and a moist band in the low troposphere behind the wake low (see their Figs. 16, 19, 22b and 25). Fig. 4 herein exhibits that a shallow precipitating cloud has formed behind the wake low by 0800 UTC. Its vertical extent was again limited by the tilted descending rear-inflow jet. Radar echo analyses by Rutledge et al. (1988) and Johnson and Hamilton (1988) also indicate the development of weak and shallow convective cells behind the wake low.

3. Three-dimensional flow structure and air trajectories

After showing the vertical cross-sectional features normal to the line, it is necessary to briefly discuss some pertinent *full* three-dimensional flow structure, particularly its alongline variability associated with the squall system.

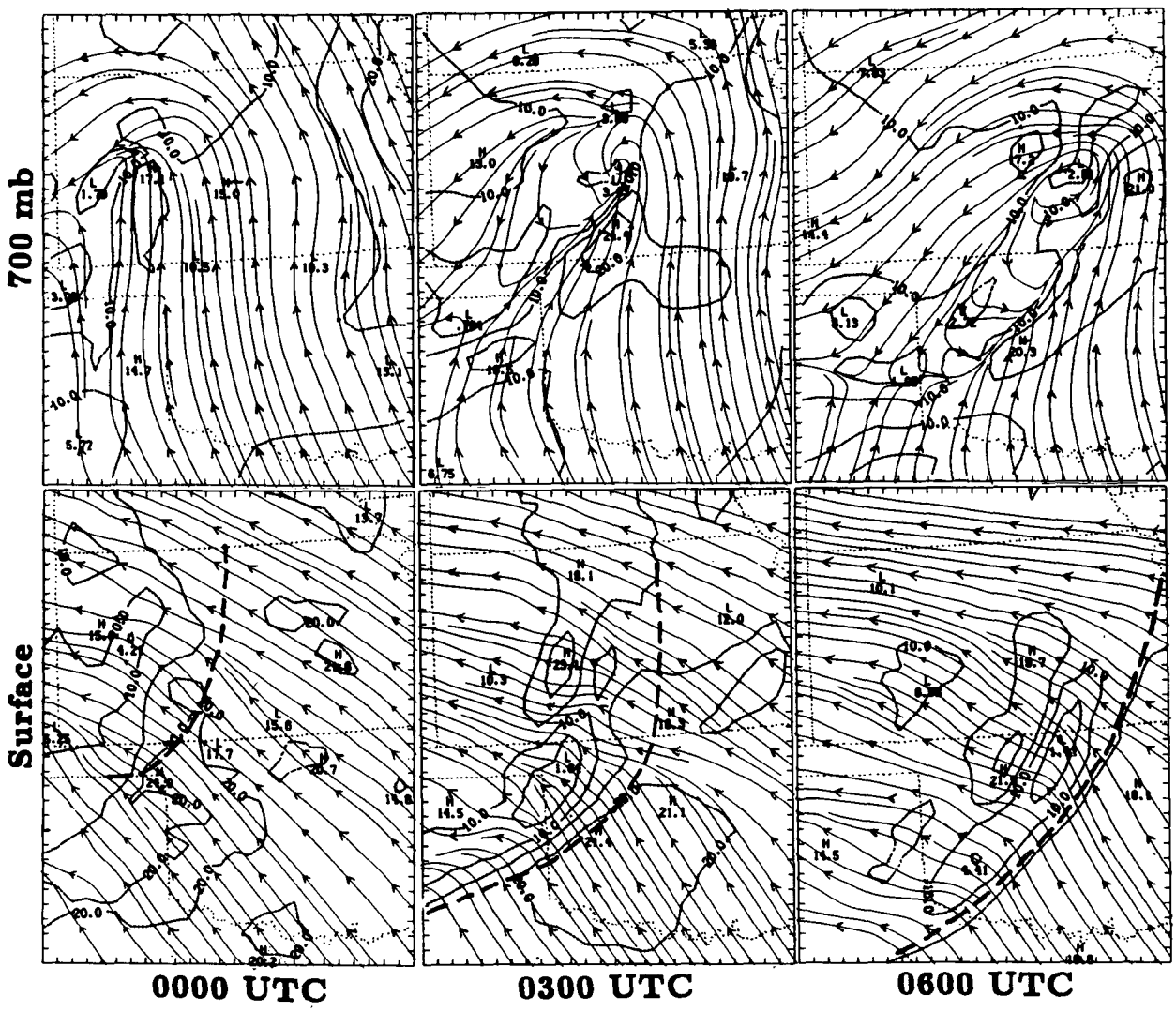

FIG. 7. (*Continued*)

a. Evolution of horizontal flow

Figure 7 summarizes mesoscale relative flow streamline analyses at 200, 400, 700 mb and the lowest σ level (about 20 m above the ground) during the intensifying and mature stages (i.e., 0000, 0300 and 0600 UTC). These levels are chosen because they are the levels where the strongest outflow (200 mb) and rear inflow (400 mb), the evolution of three distinct currents and vortex circulation (700 mb) and low-level wind shear conditions can be best described. The prestorm three-dimensional actual winds have been shown by ZGP (see their Fig. 3), that exhibited basically a SW–NE oriented troughlike flow pattern associated with a mesoα-scale short wave with an upper-level jet stream located much farther to the north and ahead of the trough axis. By 0000 UTC, the southern portion of the upper-level jet has approached the network, and has been substantially perturbed by the development of the squall line (i.e., the "blocking" effect). A very deep and extensive low-to-midlevel FTR relative inflow component was entering the squall line with winds veering with height. The dominant southerly relative flow component at upper levels was consistent with the development of extensive trailing stratiform clouds to the north of the system (see satellite imagery in ZGP). At 700 mb, a vortexlike circulation accompanying the northern segment of the line began to enter the network. At the surface, southeasterly flow with its magnitude larger than 20 m s^{-1} was approaching the squall system, and strong convergence occurred near the leading line.

During the mature stage (i.e., 0300 UTC), the model produced dramatic low-level wind perturbations as-

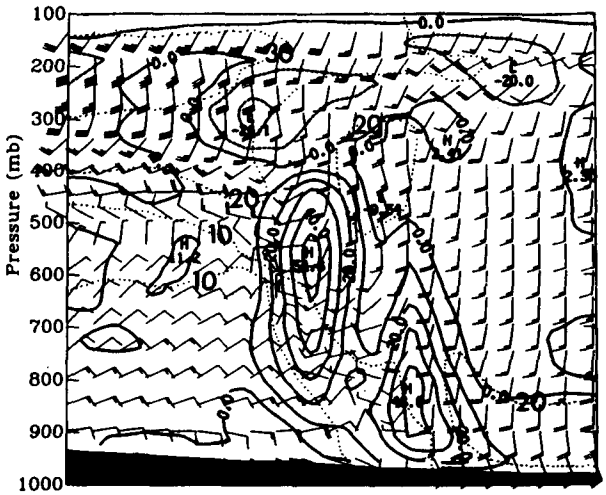

FIG. 8. Vertical cross section of horizontal relative winds (speed, m s^{-1}; direction, common convention) and relative vorticity [solid (dashed) lines are cyclonic (anticyclonic)] at intervals of 10^{-4} s^{-1} from the 18 h simulation, verified at 0600 UTC 11 June. Dotted lines are isotachs at intervals of 10 m s^{-1}. A full barb is 10 m s^{-1}. Cross sections are taken along a line as given in Fig. 1 and cover a horizontal size of 475 km.

sociated with the surface pressure perturbations. The surface easterly flow displayed a pronounced acceleration between the surface mesohigh and wake low (i.e., changed from about 10 m s^{-1} to 23 m s^{-1}), followed by a marked deceleration after having passed the wake low (i.e., from 23 m s^{-1} back to 10 m s^{-1}). It is evident that such strong convergence and divergence could considerably perturb atmospheric conditions over the wake region. At 700 mb, the mesovortex became clearly apparent to the north of the squall system. The major portion of the system consists of three distinct horizontal currents: a southerly FTR flow ahead of the line, a narrow band of the RTF flow beneath the stratiform region and a northeasterly vortex returning flow to the rear and north of the system. The vortex circulation was maximized at 600 mb and quickly vanished higher up (see Fig. 5) due to the net latent warming. At 400 mb, an extensive area of the rear inflow normal to the line was distributed behind the line, and strong convergence of the southwesterly and southeasterly flow occurred within the stratiform region (i.e., along the previously mentioned interface). The convergence line was evidently seen sloping downward from 400 mb to the surface leading line, about 150 to 200 km between. Near the tropopause, a well-developed anticyclonic circulation was centered over the stratiform region. This too indicates that the present squall line was three-dimensional in nature. Much stronger outflow developed behind the line than ahead of it, in agreement with the cross-sectional analyses presented in the last section.

At 0600 UTC, the entire tropospheric flow became well organized along the line, particularly, the low-to-midlevel convergence and the upper-level divergence. The RTF flow at 700 mb with variable intensity was well distributed over a 450 km segment along and behind the line, conforming to the Johnson and Hamilton analysis. The rear inflow at 400 mb veered inertially with time, from southwesterly at 0000 UTC to nearly westerly at this time. Thus, the normal-line component of the rear inflow was enhanced.

b. *Vertical cross section of horizontal flow*

To shed more light on the three-dimensional flow structure, Fig. 8 shows the vertical cross section of the relative flow on the same vertical plane as that in Fig. 3c for 0600 UTC, and Fig. 9 shows the time–height cross section of the relative flow for McPherson, Kansas between 0000 and 0900 UTC. In ZGP, the McPherson time–height actual wind profiles have been shown to conform remarkably well to Doppler-profiler winds analyzed by Augustine and Zipser (1987). Substantial vorticity concentration associated with the mesovortex produced a directional shear up to 500 mb. In correspondence to the convergence distribution, vertical vorticity also tilted rearward along the interface between the FTR and RTF flow. According to Zhang and Fritsch (1988b), this vertical tilt appears to partly explain why a well-defined hydrostatic surface mesolow associated with the vortex did not form in either the observations or the simulation. The most intense vortex circulation was clearly located within stratiform region (at 600 mb); another cyclonic vorticity center at 850 mb was associated with the pre-squall mesolow. The flow veered with height ahead of the rear-inflow jet and

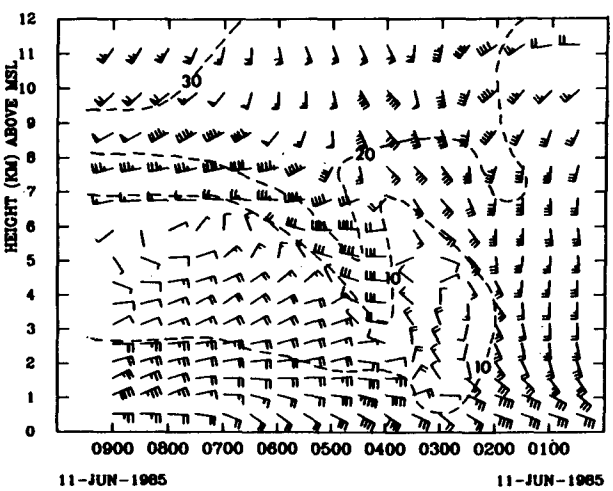

FIG. 9. The time evolution of the simulated relative wind profiles (speed, m s^{-1}; direction, common convection) at McPherson, Kansas between 0000 and 0900 UTC 11 June. Dashed lines denote isotachs at intervals of 10 m s^{-1}. A full barb is 5 m s^{-1}.

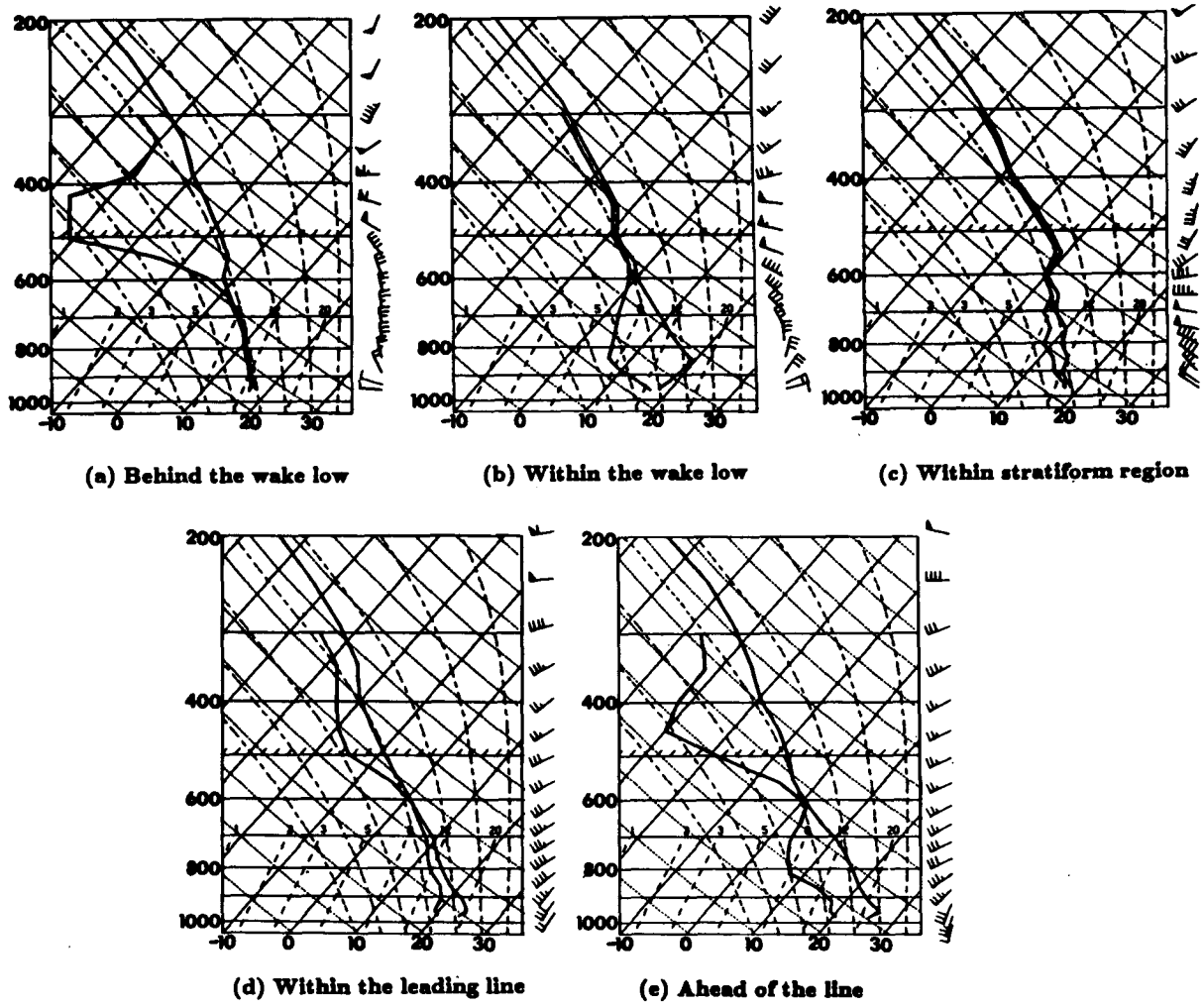

FIG. 10. Skew T–log p plot of vertical soundings taken along the cross section given in Fig. 1 from 18 h simulation, verified at 0600 UTC 11 June. A full barb is 5 m s^{-1}.

backed with height behind and beneath the rear-inflow jet. The wind flowed into the line from the front up to 400 mb and there was no steering level. Notice that the isotachs show a dipping within the rear-inflow jet. In particular, the flow direction and speed within the descending portion of the jet were quite similar to higher-level larger-scale flow behind the line and nearly decoupled with the underlying flow. This suggests that the downward transport of the upper-level high momentum by the mesoscale downdrafts may be operative. This argument would likely hold when considering that the downdraft was as strong as 1 m s^{-1}. Quantitative evaluation of the momentum transport will be reported in a future article.

c. *Vertical soundings*

Figure 10 shows a sequence of vertical soundings taken along the 0600 UTC cross-sectional plane from ahead of the line to behind the wake region, an approach similar to Smull and Houze (1987b). It is evident that the core of the strongest rear inflow dropped from 400 mb behind the wake to 700 mb at the leading edge of stratiform region. Behind the wake low (Fig. 10a), the relative humidity profile shows considerable dry air within the rear inflow with near-saturated conditions both aloft (anvil) and below (the wake convective cells). A well-known "onion-shaped" sounding (Zipser 1969, 1977) was attained within the surface wake low (Fig. 10b). We have shown in Fig. 3 that the pronounced warming and drying in this sounding can be attributed to mesoscale unsaturated downdrafts associated with the descending rear inflow. Farther forward, the stratiform region was characterized by near saturated stratification above 600 mb, and subsaturated and cool rear inflow air below (Fig. 10c). A strong wind shear appeared at the lowest levels. Apparently, both melting and evaporative cooling played an im-

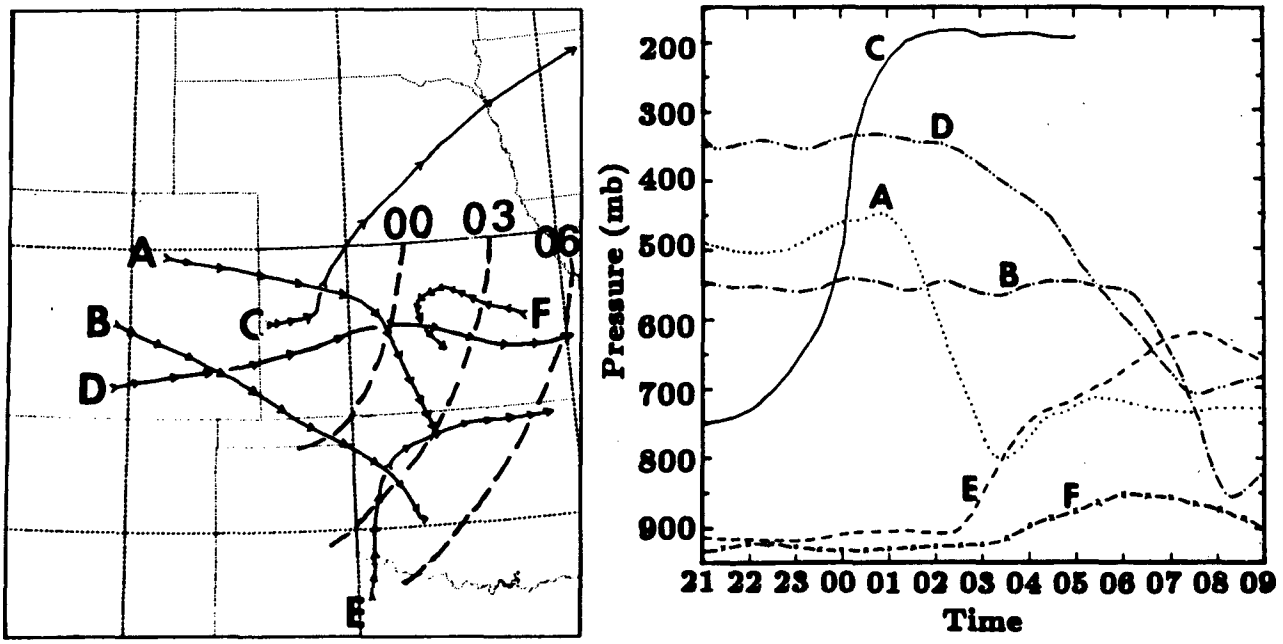

FIG. 11. (a) Horizontal projection of air trajectories between 2100 UTC 10 and 0900 UTC 11 June. Arrows and their intervals denote the directions and hourly displacement, respectively, of parcel movement. Dashed lines show the location of the simulated cold outflow associated with the squall line; (b) Vertical displacement of air parcels as a function of time.

portant role in stabilizing the stratiform region. The melting produced a 50-mb isothermal layer at 0°C with oscillatory profiles below. We consider that these features are quite realistic when compared with available observations (e.g., Leary and Houze 1979; Stewart 1984; Smull and Houze 1987b). As approaching to the leading line, the sounding showed convectively unstable conditions, but the rear inflow become less significant (Fig. 10d). However, the sounding ahead of the line at this hour was less unstable, as compared with that along the line (cf. Figs. 10d and 10e).

d. Air trajectories

As an aid in understanding the transport properties of the squall system, Fig. 11 shows six representative air trajectories that were obtained (using model-produced winds at 30-minute intervals) through forward (2100 UTC 10 to 0900 UTC 11) and backward (0900 UTC 11 to 2100 UTC 10) computations of air parcel movement. The selected parcels originated in and passed through different environments relative to the propagation of the squall line. The isochrones of cold outflow boundary at 0000, 0300, and 0600 UTC are also displayed. It is evident that as the squall line propagated eastward, it processed the low-level high-θ_e air mass from the front and over the network area, and the midlevel low-θ_e air mass from the rear and much farther west of the network within the rear-inflow jet. Thus, it appears that the one-sounding approach widely used for initiating deep convection may sometimes fail in its attempt to reproduce the right structure and evolution of MCSs when the initial conditions become crucial factors.

In general, significant vertical displacements of air parcels were highly correlated with the squall activity. Air parcels that entered the rear inflow jet sustained considerable descent and were displaced faster than the squall line. Trajectory A indicates that a 350 mb downward displacement could be realized within 2.5 hours. After reaching their lowest elevation, air parcels were carried into the wake region through the overturning downdraft, and then destabilized by the wake low (e.g., trajectories A, B, and D). The trajectory of parcel C was initially located near the place where the squall line was initiated. It appeared to be trapped within the leading updraft and quickly displaced into the upper-level layers affected by the jet stream. By 0500 UTC, this parcel was advected out of the fine-mesh domain. Air parcels that originated at the low levels ahead of the line (i.e., trajectories E and F) generally experienced slow upward motion as the squall system approached. Combined with Fig. 27 in ZGP, the displacement of trajectory E before 0300 UTC suggests that the northward advection of the convectively stable, deep south-to-southwesterly flow (see Fig. 3 in ZGP) played an important role in rapidly suppressing convective activity along the leading line.

4. Effects of latent cooling and water loading

Since the simulation showed a close relation of the development of the surface pressure perturbations and

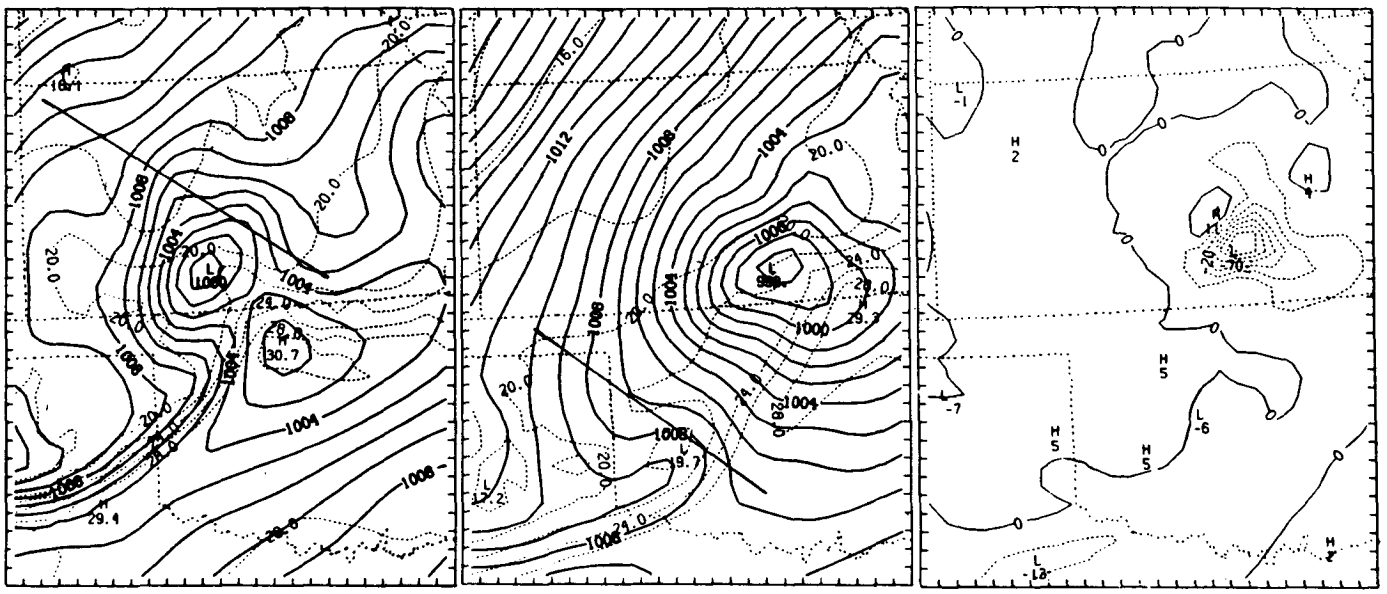

FIG. 12. (a), (b) Simulated evolution of sea-level pressure (solid lines, mb) and surface temperature (dashed lines, °C) for Expt. NEV (no evaporation) from 15 and 18 h simulations, verified at 0300 and 0600 UTC 11 June, respectively. (c) Simulated 850 mb vertical motion (ω, μb s^{-1}) for 0600 UTC 11 June.

descending rear-inflow jet to the latent cooling, this simulation will be utilized in this section as a control run (Expt. CTL) to examine the model's sensitivity to evaporative cooling, ice microphysics, hydrostatic water loading and parameterized moist downdrafts. The methodology adopted here is similar to that presented in Zhang et al. (1988), Zhang and Fritsch (1988a) and Zhang (1989) for the study of the 1977 Johnstown MCSs. In that case, each experimental simulation was conducted with conditions identical to the control run except for the treatment of the above individual model physics. In general, the effects of those physics on the generation of the wake low and descending rear inflow can be evaluated by directly examining surface pressure perturbations, the normal-line flow component and the vertical motion. Details of these experimental simulations are discussed below.

a. Effect of resolvable-scale evaporative cooling

When resolvable-scale evaporation and sublimation were omitted (Expt. NEV), the model produced a different evolution as compared to the control. In particular, the simulated squall system did not possess the significant line structure, such as the elongated presquall mesolow, mesohigh, wake low and vertical motion band as that produced by Expt. CTL (cf. Figs. 15, 16 and 19 in ZGP and Fig. 12 herein). A strong surface mesolow developed behind and to the north of the leading line. Unlike the wake low in the control run, this low was not produced by subsidence warming but by a positive feedback process among latent heat release, low-level mass and moisture convergence, and surface pressure falls that was associated with the mesovortex. This is a runaway CISK-like instability exactly as that discussed by Zhang et al. (1988). In that paper, it was also found that, without the retarding effect of the evaporative cooling, the Johnstown mesolow/mesovortex sustained unrealistic intensification of vertical motion and spinup of cyclonic vorticity. As shown in ZGP and Fig. 1 herein, neither observations nor Expt. CTL exhibited the formation of the surface mesolow in relation to the mesovortex. By 0600 UTC, this mesolow merged with the presquall mesolow, and the squall system was dominated by the extensive vortex circulation. Strong upward motion developed near the center of the vortex (see Figs. 2, 12 and 13); its magnitude almost doubled compared to that in Expt. CTL. By contrast, the model produced very weak ascending motion along the line portion of the squall system in this experiment.

Perhaps one of the most profound results to Expt. NEV is that, in the absence of the resolvable-scale evaporative cooling, the rear-inflow jet was weak and did not extend downward to the surface (Fig. 13). From the discussion in section 2, this is evidently due to the failure of Expt. NEV to generate a surface mesohigh behind the leading line. Although a strong midlevel mesolow developed, it only helped enhance the low-to-midlevel convergence between the RTF and FTR

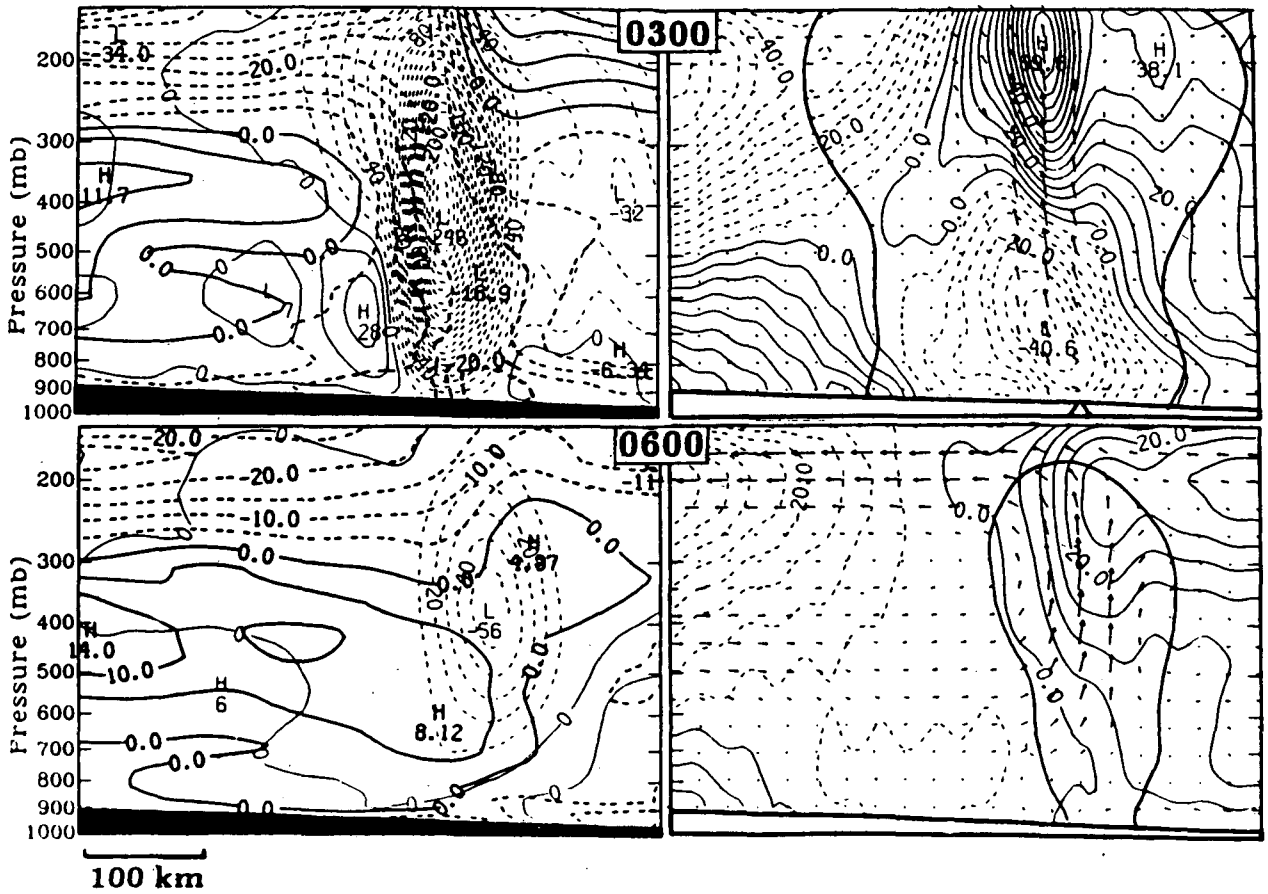

FIG. 13. As in Fig. 3 but for Expt. NEV (no evaporation) from 15 and 18 h simulations, verified at 0300 and 0600 UTC 11 June, respectively. Thick solid line at the right panel denotes rainwater content larger than 0.2 g kg^{-1}.

flow. Thus, it follows that *the midlevel mesolow mechanism proposed by Smull and Houze (1987b) cannot be used alone to explain the generation of the descending rear inflow*. The development of the strong midlevel mesolow in combination with a pronounced upper-level mesohigh led to the significant intensification of the vortex circulation. As a consequence, the upper-level FTR outflow was excessively strong and the low-level FTR flow behind the line was too weak, as compared to those in Expt. CTL. Of striking interest in Fig. 13 is that the system failed to show a significant upshear tilt over the period 0300–0600 UTC as in Expt. CTL, further supporting the RKW theory that the favorable interaction of the low-level wind shear with the convectively generated cold pool tends to produce a vigorous and longlived convective system.

b. *Effect of ice microphysics*

By removing ice microphysics from the model (Expt. NIC), the most obvious effects are the considerable weakening of surface pressure perturbations and vertical circulation for the entire convective system although the basic patterns were still similar to Expt. CTL (cf. Figs. 1 and 14). Likewise, peak updrafts and downdrafts were much weaker (Fig. 2). Both the observed and control-simulated squall–mesohigh and wake low did not materialize in this simulation. Instead, a weak mesoridge and a mesotrough developed behind the line. Meanwhile, the mesovortex was unable to be appreciably strengthened. In the simulation of the 1977 Johnstown MCSs, Zhang (1989) found that with the inclusion of ice microphysics, the commonly observed delay in the grid-box saturation could be significantly improved due to the relaxed saturation criterion. Then, as a result of additional latent heat release of fusion, the MCS would undergo a more rapid acceleration during its development stage. In the present case, most of precipitable water originated from the lower-level high-θ_e air ahead of the system (Fig. 4), and was later carried north- and rear-ward in the anvil by the FTR updrafts (Fig. 3). Thus, the neglect of the relaxed saturation at upper levels and latent heating

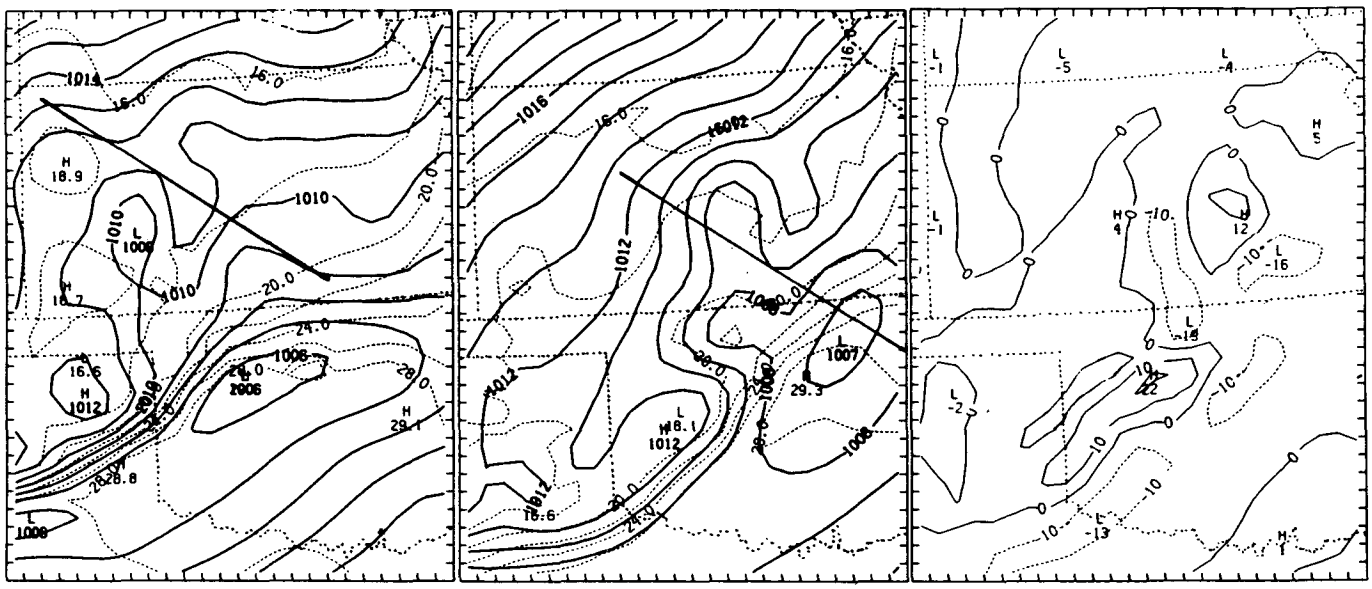

FIG. 14. As in Fig. 12, but for Expt. NIC (no ice microphysics).

by fusion as the condensate was advected upward across through the 0°C isotherm explains why the squall line in Expt. NIC was relatively weak. Moreover, since the system processed the boundary-layer high-θ_e air ahead of the line and since there is a strong southwesterly wind component at upper levels, the present squall line was driven by latent heat release (condensation plus fusion) in the front and latent cooling (evaporation and melting) to the rear and north of the system. This appears to be part of the reasons why both the observed and control-simulated mesovortex behind the line could not intensify as fully as that described in Zhang and Fritsch (1986), and also helps explain why the surface mesohigh and wake low were stronger over the northern segment of the system. When only ice melting was omitted from Expt. CTL (not shown), the magnitude and distribution of the upward motion were comparable to that in Expt. CTL but mesoscale sinking and surface pressure perturbations behind the system were similar to Expt. NIC. Lord et al. (1984) and Fovell and Ogura (1988) also noted that the incorporation of ice microphysics helps produce the realistic structure and evolution of MCSs.

Because of the generated weak surface mesohigh and weak midlevel mesolow, the rear-inflow jet only descended a little but could not reach close to the ground (Fig. 15). Although the three distinct airflows were reasonably reproduced, their magnitudes were all small, particularly for mesoscale downdrafts within the rear inflow. Thus, the height deviations differed markedly from the control run in both distribution and magnitude.

c. *Effect of parameterized moist downdrafts*

The effect of parameterized moist downdrafts were excluded from the Fritsch–Chappell convective scheme in the same way as that presented in Zhang and Fritsch (1989). Without the parameterized downdrafts (Expt. NPD), the squall system propagated more slowly, and lagged about 150 km (equivalent to three hours) behind the control-simulated (Fig. 16). This slowness, coupled with relatively strong convective forcing, led to an enhanced pressure gradient across the leading line. Like previous experimental simulations, a strong surface mesolow developed near the leading line as a result of the intensification of the mesovortex. To the rear of the system, the neglect of the downdraft cooling resulted in a weak mesohigh and a weak wake low by 0600 UTC. Interestingly, when the Anthes–Kuo type of the convective parameterization scheme (Anthes et al. 1987) was utilized for both nested-grid meshes, the model failed to reproduce the squall line and needless to say, the surface mesohigh and wake low. This difference appears to be associated with the value of the b parameter in the Anthes–Kuo scheme being too large to produce strong enough mass perturbations for the continued development of deep convection, as is often the case (see Zhang and Fritsch 1988a for the related discussion).

Based upon the foregoing presentations, the failure to predict the surface pressure perturbation would produce an unrealistic structure of the rear inflow and midlevel pressure perturbations. Apparently, the effect of the parameterized downdrafts is to help enhance the

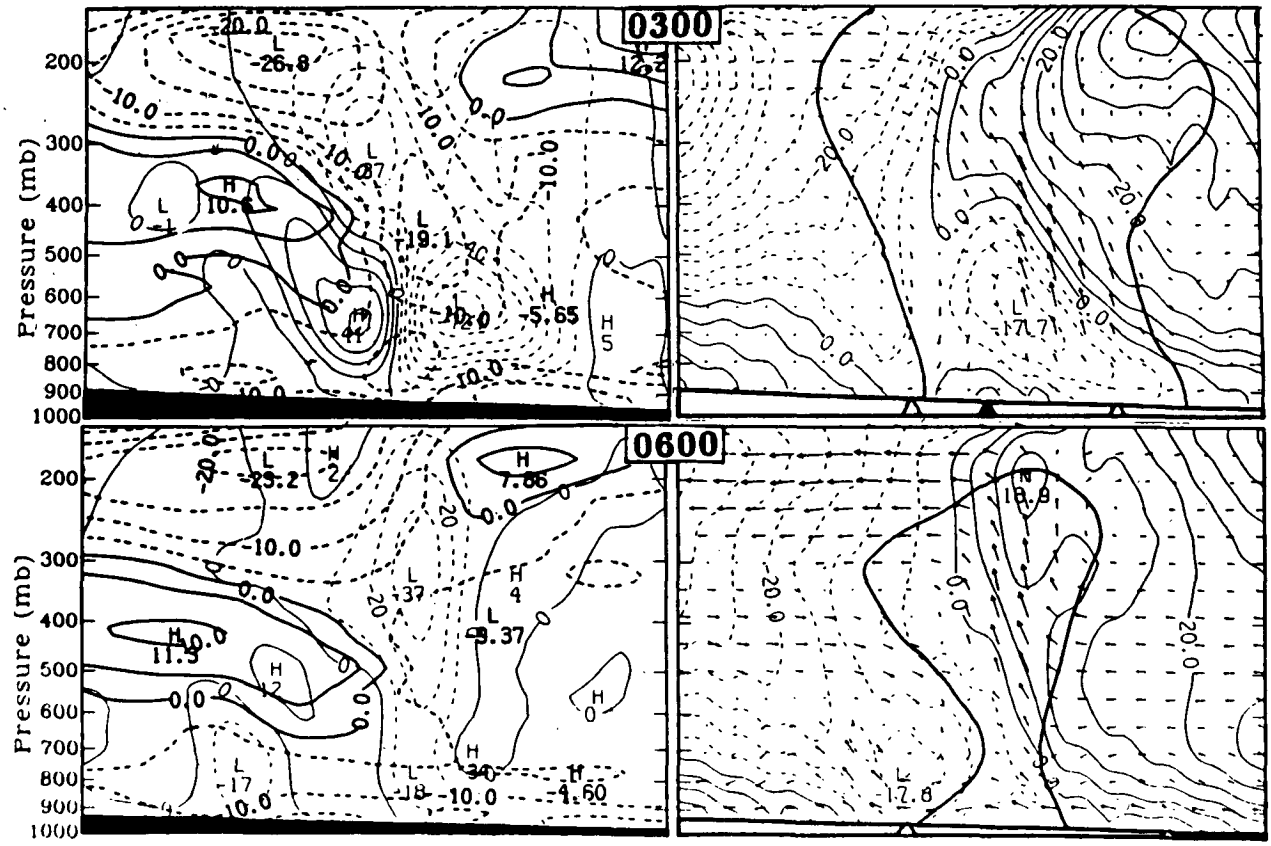

FIG. 15. As in Fig. 3, but for Expt. NIC (no ice microphysics) from 15 and 18 h simulations, verifying at 0300 and 0600 UTC 11 June, respectively. Thick solid line at the right panel denotes rainwater content larger than 0.2 g kg^{-1}.

surface mesohigh for the development of the descending rear inflow and the lifting of high-θ_e air in the FTR current to the condensation level, thereby rapidly generating new convection ahead of the line. Another effect is to produce a "brake" on the development of the CISK-like instability by incorporating lower-θ_e air into

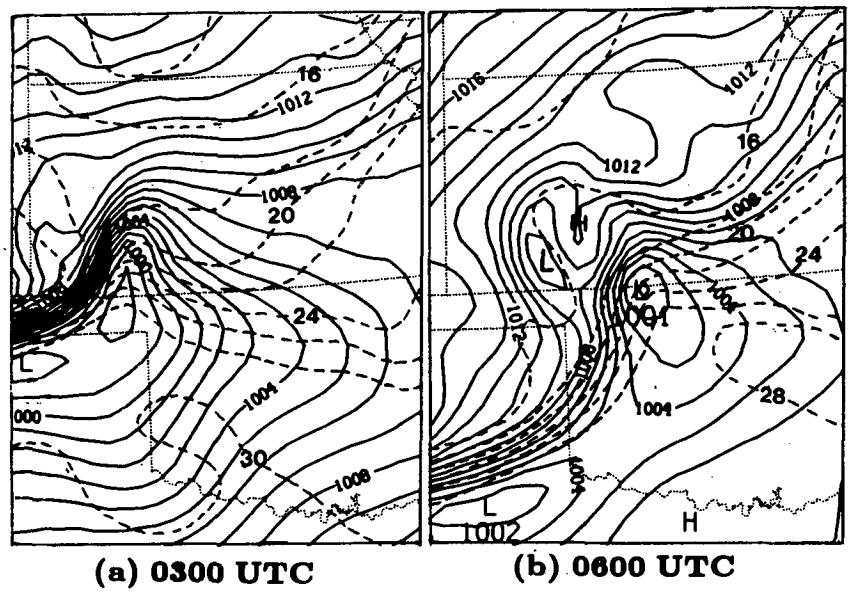

FIG. 16. As in Fig. 12, but for Expt. NPD (no parameterized downdrafts).

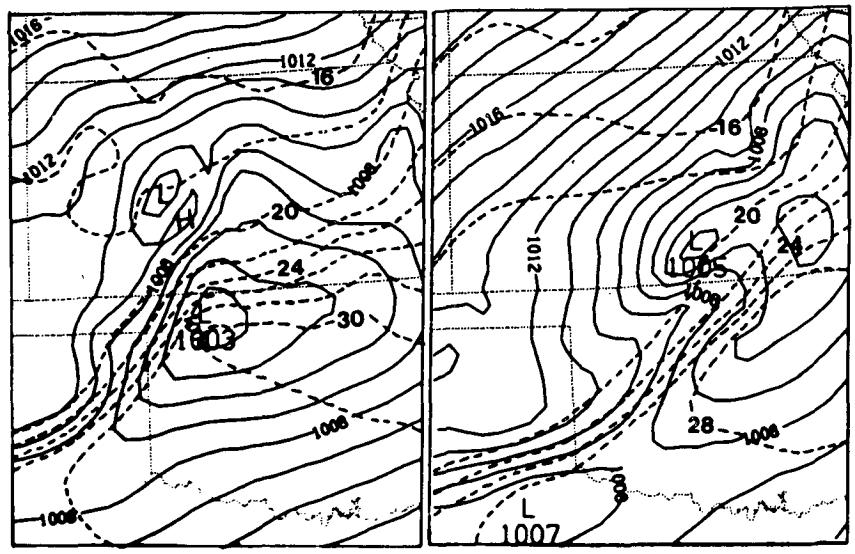

FIG. 17. As in Fig. 12, but for Expt. WWL (weak water loading).

the boundary layer and producing a weaker upper-level mesohigh. Thus, when the parameterized downdrafts are activated in the model, the convective system would be forced to move ahead, and the peak updrafts would be retarded. A similar conclusion was also reached by Zhang and Fritsch (1988a) for the simulation of the 1977 Johnstown MCSs.

d. Effect of weak water loading

As discussed in ZGP, terminal velocities of raindrops and snow in Expt. CTL were subjectively reduced by 70% because they were originally calculated using formulae commonly used by nonhydrostatic cloud models with a grid size much less than 5 km (see Zhang 1989). This change is an attempt to realistically account for the effect of hydrostatic water loading in nature. That is, the smaller the terminal velocity is, the longer time the condensate will stay in an atmospheric column, and thus the water loading will be enhanced. The water loading tends to affect the atmospheric circulation by compensating for the virtual temperature effect in the calculation of the geopotential height, thus indirectly retarding updrafts (see Zhang et al. 1988).

Without the 70% reduction in the terminal velocity (Expt. WWL), the model also predicted a deeper presquall mesolow, a weaker mesohigh and a weaker wake low behind the system (Fig. 17), as did in previously discussed experimental simulations. As we could anticipate, the descending rear inflow jet could not possibly be well developed (not shown). When the water loading was completely ignored in computing the geopotential height, tremendous spinup of the vortex occurred; the surface mesolow was deeper than that in Expt. NEV (not shown). Zhang et al. (1988) also found such overenhancement of the vortex circulation when the water loading effect was totally neglected.

5. Scale interaction

From the experimental simulations, it appears that latent cooling and water loading are responsible for the realistic generation of the surface mesohighs, the ultimate descent of the rear-inflow jet to the surface, and indirectly the surface wake lows. In all the simulations, there were always strong trailing rear inflow present in the midtroposphere regardless of the formation of the surface mesohighs and wake lows. Therefore, a question is: Did the strong rear inflow develop as a consequence of intense large-scale environmental winds overtaking the system, or as a dynamic response to the development of the squall line? Our model results shown below suggest that there were three different scales of dynamic processes involved in the development of the present rear inflow jet.

Figures 18a and 18b show the 18 h simulated surface pressure and temperature, and the cross-sectional analysis of relative winds and circulation vectors, respectively, verified at 0600 UTC, from a simulation in which neither convective nor resolvable-scale condensation effects are included (Expt. NDH, see Zhang and Fritsch 1988a for further description). The cross section was taken along the same vertical plane but at a larger scale (with the horizontal span of 900 km) than that used in the preceding sections. This experiment presumably represents the "true" evolution of the undisturbed large-scale environment without the influence of the squall line. By turning off diabatic heating, par-

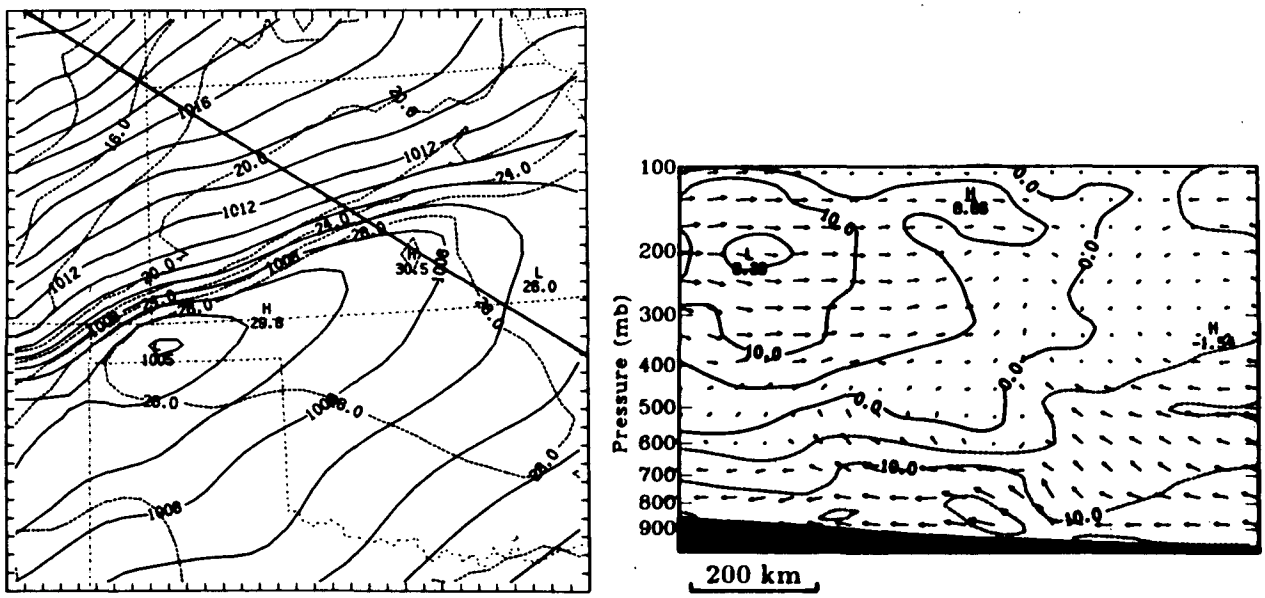

FIG. 18. (a) As in Fig. 12, but for Expt. NDH (no diabatic heating) from 18 h simulation, verified at 0600 UTC 11 June; (b) NW-SE vertical cross-sectional distribution of relative flow and circulation vectors (normal to the line) at intervals of 5 m s^{-1} from the 18 h simulation (see Fig. 18a for the location). Solid (dashed) lines denote RTF (FTR) flow. The cross section covers a horizontal size of 900 km.

ticularly the moist downdraft effects, the surface front propagated too slowly, at least 300 km behind the control-simulated. Meanwhile, the peak upward motion along the front (not shown) was much weaker (≤ 10 μb s^{-1}) although it was not strong to begin with. As mentioned in ZGP, continued downslope adiabatic warming over the Rocky Mountains and boundary layer development contributed to the weakening of the frontal system.

In spite of the obvious effects of neglecting the development of the MCS, Expt. NDH still clearly shows a deep layer of strong RTF flow in the upper troposphere to the rear of the system, and a FTR current below 600 mb. As previously mentioned, this strong RTF flow was associated with an upper-level jet stream to the north of the network. Thus, it has a horizontal scale close to the half wavelength of the mesoα-scale short wave. This indicates that the large-scale baroclinity provided a persistent and favorable RTF flow component for the development of the present squall system.

In order to better examine the relative importance of the squall system versus the large-scale baroclinity in determining the vertical flow structure, Fig. 19a displays the vertical distribution of relative flow from the control run along the same cross section and for the same hour as Fig. 18b, and Fig. 19b shows the resulting difference field between Expts. CTL and NDH (i.e., relative speed in Fig. 19a minus that in Fig. 18b). It is apparent that the squall line accounted for the generation of the intense FTR outflow at the upper levels and the strong descending RTF motion behind the line. The shallow convective cells over the wake region appear to be responsible for another rear inflow perturbation to the left. There was little influence of the MCS on the environmental flow ahead of the system. Of primary concern here is to determine how the strong and extensive trailing rear inflow around 400 mb was generated. Fig. 19b shows a speed difference of only about 6–7 m s^{-1}, suggesting that the squall line was responsible for at most 50% of the intensity of the trailing rear inflow. Even for this percentage, it may be related to the large-scale environmental wind structure. Specifically, downward momentum transport by the upper-level convergence at the back edge of the FTR outflow would help intensify the trailing rear inflow.

The above result does not contradict the conclusion reached by Smull and Houze (1987b) and Lafore and Moncrieff (1989) that rear inflow develops basically as a response to processes occurring within MCSs, since the rear inflow they resolved is more or less the descending portion of the rear inflow as in the present case. In fact, when relative flow deviations normal to the line were constructed from Fig. 19a by subtracting its five-hour running average (Fig. 19c), the most obvious remaining feature is the descending portion of the rear inflow; it occupied more than a 300 km horizontal region to the rear of the line. This reveals that both the midlevel trailing rear inflow and the upper-level FTR outflow are on time and space scales much larger than the descending portion of the rear inflow. Therefore, we have demonstrated that there were three different scales of atmospheric motion interacting in the development of the present rear inflow: *the large-scale baroclinity produced the strong RTF flow within the upper half of the troposphere, the mesoscale response*

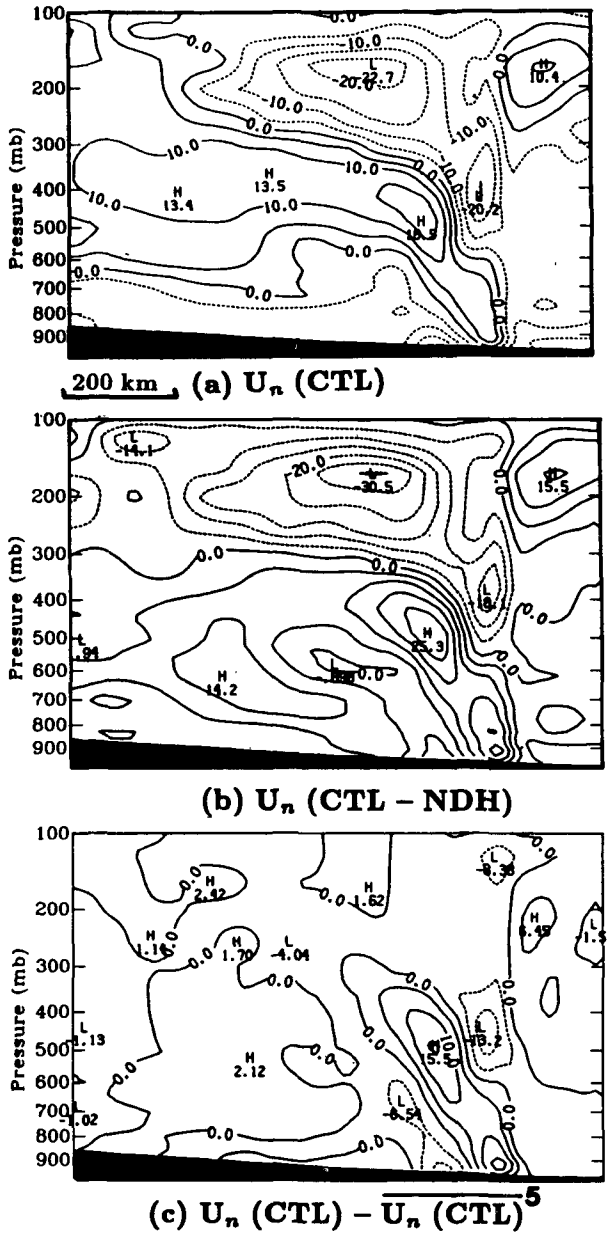

FIG. 19. (a) As in Fig. 18b, but from Expt. CTL (control run); (b) The vertical cross section of the normal-line difference speed between Expts. CTL and NDH along the same line as for Fig. 18b for 0600 UTC; (c) The vertical cross section of speed deviations over its five-hour running average from the 18 h control simulation along the same line as for Fig. 18b.

to the convective development enhanced the midlevel trailing rear inflow, and the moist downdrafts was responsible for the descending portion of the rear inflow close to the leading line. It can be speculated that without the large-scale baroclinic support, both the rear-inflow jet and the surface wake low in the present case would not be so strong nor the squall line so intense. Furthermore, the development of different intensity of the above three processes helps explain why squall lines sometimes produced "the strong rear inflow," sometimes generated "the weak rear inflow," or sometimes resulted in "the stagnation zone" (see Smull and Houze 1987b for the classification).

To gain insight into the effect of the squall system on the larger-scale thermodynamic environment, Figs. 20a and 20b display the simulated difference fields of respective θ_e and temperature between Expts. CTL and NDH for 0600 UTC. It is apparent that the squall line derived the high-θ_e air from the boundary layer, transported it into the upper troposphere for the generation of stratiform clouds, and then left behind much low-θ_e air in the low troposphere, thereby stablizing the atmosphere. Note that the descending rear inflow is just located along the leading edge of the low-θ_e pool, suggesting that its kinetic energy was converted from potential energy through the gravitational overturning processes, and *the descending rear inflow is a product of the dynamic response to the latent-cooling-induced circulations.* The squall system produced 7°–8°C net warming within the stratiform region and 6°–9°C

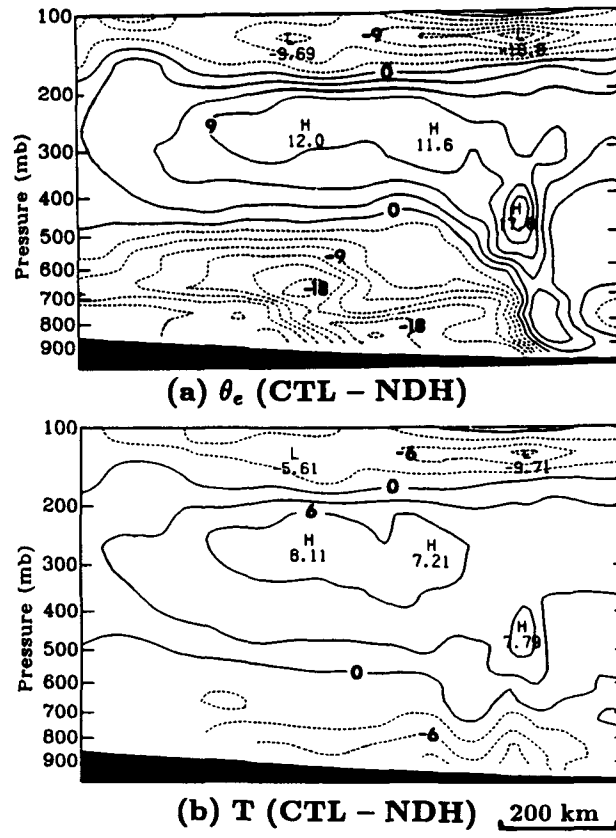

FIG. 20. The vertical cross section of the (a) difference θ_e at intervals of 3 K and (b) the difference temperature at intervals of 3°C between Expts. CTL (control run) and NDH (no diabatic heating) along the same line as for Fig. 18b from 18 h simulation, verified at 0600 UTC 11 June.

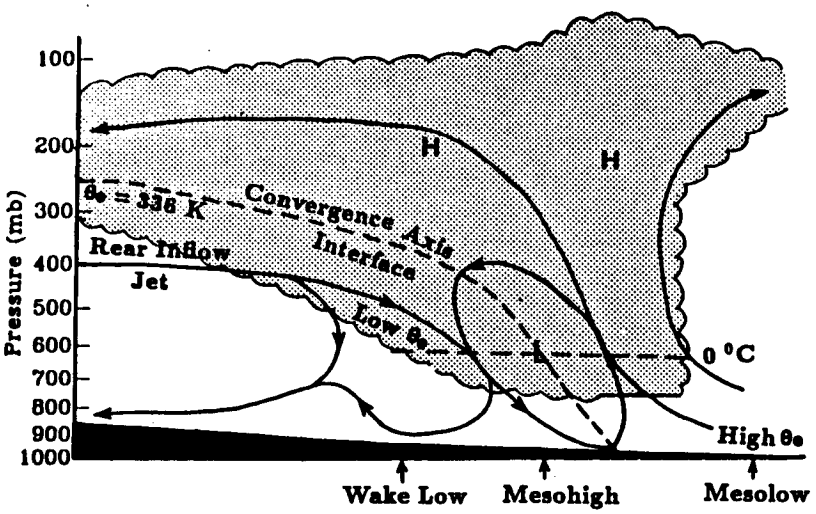

FIG. 21. A conceptual model of the simulated storm-relative airflows, tropospheric and surface pressure perturbations during squall system mature stage. Arrows denote streamlines, not trajectories.

cooling below, which accounted for about 70% and 40%, respectively, of the θ_e changes. This indicates that the drying by the descending rear inflow and parameterized convection far exceeded the moistening by evaporation in the lower half of the troposphere. At the upper levels, convective heating was the major effect of the squall line on the large-scale environment.

6. Summary and concluding remarks

In this paper, an intense rear-inflow jet, surface pressure perturbations and stratiform precipitation associated with the 10–11 June 1985 PRE-STORM squall line have been examined through the use of a three-dimensional mesoscale hydrostatic model. The squall line was initiated when a southeasterly propagating cold front encountered a convectively unstable thermal boundary to the west of the network. Later, continued latent heat release strengthened the leading updrafts, and the resulting large amount of upward mass transport produced strong outflow at the upper levels and interrupted the midlevel rear-to-front flow. Thus, rear inflow was formed behind the line. However, the descent of the rear inflow did not commence until a surface mesohigh and a midlevel mesolow materialized and forced air within the rear inflow to subside. This midlevel mesolow, which was located near the level of the 0°C isotherm, could be attributed to melting and evaporative cooling below latent heating. Until the surface mesohigh fully developed, the resulting strong rear-to-front outflow was overtaken by the subsiding rear inflow to form the deep descending flow which extended forward and downward into the leading updrafts. As the considerable amount of air within the rear inflow sank and as the subsidence warming and drying overwhelmed melting and evaporative cooling and moistening toward the rear, a surface wake low began to form at the back edge of the system. Because of pronounced mass evacuation in the low troposphere, air parcels tended to become dynamically destabilized over the wake region. However, its upward penetration was limited by the intense rear inflow of dry air. The drying effect of the rear inflow has been shown by air trajectories which underwent a 350 mb downward displacement within 2.5 hours. These mesoscale features diminished as the system moved into a convectively unfavorable environment.

As an aid in describing the structure of the squall system, Fig. 21 shows a conceptual model constructed from the model results during the mature stage. There are three distinct airflow branches within the system: a leading overturning updraft and an ascending front-to-rear updraft that both were driven by high-θ_e air from the boundary layer ahead of the system, and an overturning downdraft carrying low-θ_e air from the rear. A rotor within the stratiform region indicates the interaction of the dry and cold rear inflow with the leading updrafts. Due to continuous deposit of front-to-rear momentum at the upper levels, the front-to-rear penetrative updraft is responsible for the rearward transport of high-θ_e air mass for the generation of the trailing stratiform precipitation. Several pressure perturbations developed in relation to these flow structures. For example, there existed two mesohighs at the upper levels: one was produced by the leading updrafts, and another was near the heart of the stratiform region and responsible for the continuous light rainfall behind the line. Between these two mesohighs was weak vertical motion with an underlying transition zone. Notice that the midlevel pressure and divergence troughs coincided with the interface between the rear-inflow jet and the front-to-rear current, and also demarcated mesoscale

updrafts and downdrafts. Behind the midlevel mesolow and the underlying surface mesohigh was a rearwardly tilted wake low (trough) that was produced by subsidence warming in the unsaturated downdrafts. The core of the rear inflow was located halfway between the low pressures, and extended to ahead of the surface mesohigh. The wake low was located at the place where the sinking persisted the longest. The above features have been shown to be well distributed over a 450 km segment parallel to and behind the leading line.

Experimental simulations indicate that the large-scale baroclinity provided deep and favorable rear-to-front flow within the upper half of the troposphere. The mesoscale response to convective forcing enhanced the trailing rear inflow while latent cooling and water loading were directly responsible for the generation of the descending portion of the rear inflow. The previously proposed midlevel mesolow mechanism cannot be used alone to explain the generation of the descending rear inflow. The effects of the moist downdrafts appear to help (i) deepen the surface mesohigh for the generation of the descending rear inflow; (ii) strengthen the low-level convergence near the leading line and thereby cause dynamic lifting; and (iii) retard the development of the vortex circulation so as to reduce the transport of low-θ_e air from the rear of the system into the convective portion of the line. Furthermore, the incorporation of reasonable downdraft properties tends to help reproduce the realistic structure and lifecycle of the squall system, e.g., the generation of stratiform rainfall, relative flow, and downshear/upshear tilts. Although both the resolvable-scale and parameterized cooling are responsible for generating the low-level cold pool (mesohigh), they appear to have played a different role in the development of the descending rear inflow. This is because the resolvable-scale cooling occurs kinematically and thus tends to carry the upper and mid-level high momentum downward, whereas the parameterized downdrafts produce collective low-level cooling for intensifying cold outflow and help the rear inflow extend downward and forward near the leading convection. In particular, we feel that without the resolvable-scale cooling mechanism, the rear inflow in the present case could not possibly descend from 400 mb to near the surface unless the surface mesohigh was unrealistically deep and intense.

In general, the role of the rear-inflow jet is to produce convergence ahead and divergence behind. Thus, strong rear inflow helps accelerate and strengthen the leading convective activity when entering a convectively favorable environment. Otherwise, it tends to aid the rapid dissipation of the squall system. This finding is consistent with the Rotunno et al. (1988) theory in which cold pool plays different roles in determining the circulation structure of squall lines during the lifecycle. Stronger descending rear inflow also helps produce a more intense surface wake low behind. Our simulation illustrates that the surface wake low can be considered as an end product of complicated reactions from condensate production to latent cooling, the intensified descending rear inflow, and strong warming and drying. It did not appear to have any significant effects on atmospheric features developed ahead, but was responsible for the dynamic destabilization of the wake region.

The results indicate that numerical models can be a very useful and effective tool in mesometeorology for supplementing and extending observations (Keyser and Uccellini 1987). The results also indicate that reasonable model physics such as ice microphysics, convective parameterizations and resolvable-scale phase changes are essential for reproducing the realistic mesoβ-scale structure and evolution of MCSs even with the conventional meteorological observations.

Acknowledgments. We would like to thank G. Barnes, C. Doswell III, M. Moncrieff, B. Smull, and M. Weisman for their helpful comments on this manuscript. We benefitted from discussions with J. M. Fritsch, J. Klemp, P. LeMone, R. Rotunno, and E. Zipser. We are grateful to the Mesoscale and Microscale Meteorology Division and the Advanced Study Program, NCAR for sponsoring this research and for the computer support during the course of this study. The computations were performed at the NCAR CRAY X-MP.

REFERENCES

Anthes, R. A., E.-Y. Hsie and Y.-H. Kuo, 1987: Description of the Penn State/NCAR mesoscale model version 4 (MM4). NCAR Tech. Note, NCAR/TN-282, 66 pp.

Augustine, J. A., and E. J. Zipser, 1987: The use of wind profilers in a mesoscale experiment. *Bull. Amer. Meteor. Soc.*, **68**, 4–17.

Brown, J. M., 1979: Mesoscale unsaturated downdrafts driven by rainfall evaporation: A numerical study. *J. Atmos. Sci.*, **36**, 313–338.

Chong, M., P. Amayenc, G. Scialom and J. Testud, 1987: A tropical squall line observed during the COPT 81 experiment in West Africa. Part I: Kinematic structure inferred from dual-Doppler radar data. *Mon. Wea. Rev.*, **115**, 670–694.

Cunning, J. B., 1986: The Oklahoma–Kansas Preliminary Regional Experiment for STORM–Central. *Bull. Amer. Meteor. Soc.*, **67**, 1478–1486.

Fovell, R. G., and Y. Ogura, 1988: Numerical simulation of a mid-latitude squall line in two dimensions. *J. Atmos. Sci.*, **45**, 3846–3879.

Fritsch, J. M., and C. F. Chappell, 1980: Numerical prediction of convectively driven mesoscale pressure systems. Part I: Convective parameterization. *J. Atmos. Sci.*, **37**, 1722–1733.

Gamache, J. F., and R. A. Houze, Jr., 1982: Mesoscale air motions associated with a tropical squall line. *Mon. Wea. Rev.*, **110**, 118–135.

Hamilton, R. A., and J. W. Archbold, 1945: Meteorology of Nigeria and adjacent territory. *Quart. J. Roy. Meteor. Soc.*, **71**, 231–264.

Houze, R. A., Jr., 1977: Structure and dynamics of a tropical squall-line system. *Mon. Wea. Rev.*, **105**, 1540–1567.

Johnson, R. H., and P. J. Hamilton, 1988: The relationship of surface pressure features to the precipitation and air flow structure of

an intense midlatitude squall line. *Mon. Wea. Rev.*, **116,** 1444–1472.

Keyser, D., and L. W. Uccellini, 1987: Regional models: Emerging research tools for synoptic meteorologists. *Bull. Amer. Meteor. Soc.*, **68,** 306–320.

Lafore, J.-P., and M. W. Moncrieff, 1989: A numerical investigation of the organization and interaction of the convective and mesoscale regions of tropical squall lines. *J. Atmos. Sci.*, **46,** 521–544.

Leary, C. A., and R. A. Houze, Jr., 1979: Melting and evaporation of hydrometers in precipitation from anvil clouds of deep tropical convection. *J. Atmos. Sci.*, **36,** 669–679.

——, and E. N. Rappaport, 1987: The life cycle and internal structure of a mesoscale convective complex. *Mon. Wea. Rev.*, **115,** 1503–1527.

LeMone, M. A., 1983: Momentum transport by a line of cumulonimbus. *J. Atmos. Sci.*, **40,** 1815–1834.

——, G. M. Barnes and E. J. Zipser, 1984: Momentum flux by lines of cumulonimbus over the tropical oceans. *J. Atmos. Sci.*, **41,** 1914–1932.

Lord, S. J., H. E. Willoughby and J. M. Piotrowicz, 1984: Role of a parameterized ice-phase microphysics in an axisymetric, nonhydrostatic tropical cyclone model. *J. Atmos. Sci.*, **41,** 2836–2848.

Menard, R. D., D. L. Sims and J. M. Fritsch, 1988: Case example of the effect of a wake low on subsequent convective events. Preprints, *15th Conf. on Severe Local Storms,* Baltimore, Amer. Meteor. Soc., 225–228.

Moncrieff, M. W., 1978: The dynamical structure of two-dimensional steady convection in constant vertical shear. *Q. J. Roy. Meteor. Soc.*, **104,** 543–567.

——, 1981: A theory of organized steady convection and its transport properties. *Q. J. Roy. Meteor. Soc.*, **107,** 29–50.

Newton, C. W., 1950: Structure and mechanism of the prefrontal squall line. *J. Meteor.*, **7,** 210–222.

——, 1966: Circulations in large sheared cumulonimbus. *Tellus,* **18,** 699–712.

Ogura, Y., and M. T. Liou, 1980: The structure of a midlatitude squall line: A case study. *J. Atmos. Sci.*, **37,** 553–567.

Rotunno, R., J. B. Klemp and M. L. Weisman, 1988: A theory for strong, long-lived squall line. *J. Atmos. Sci.*, **45,** 463–485.

Rutledge, S. A., R. A. Houze, Jr., M. I. Biggerstaff and T. Matejka, 1988: The Oklahoma–Kansas mesoscale convective system of 10–11 June 1985: Precipitation structure and single-Doppler radar analysis. *Mon. Wea. Rev.*, **116,** 1409–1430.

Seitter, K. L., and H.-L. Kuo, 1983: The dynamic structure of squall-line type thunderstorms. *J. Atmos. Sci.*, **40,** 2831–2854.

Smull, B. F., and R. A. Houze, Jr., 1985: A midlatitude squall line with a trailing region of stratiform rain: Radar and satellite observations. *Mon. Wea. Rev.*, **113,** 117–133.

——, and ——, 1987a: Dual-Doppler radar analysis of a midlatitude squall line with a trailing region of stratiform rain. *J. Atmos. Sci.*, **44,** 2128–2148.

——, and ——, 1987b: Rear-inflow in squall lines with trailing stratiform precipitation. *Mon. Wea. Rev.*, **115,** 2869–2889.

Stewart, R. E., 1984: Deep 0°C isothermal layers within precipitation bands over southern Ontario. *J. Geophys. Res.*, **89,** 2567–2572.

Thorpe, A. J., M. J. Miller and M. W. Moncrieff, 1982: Two-dimensional convection in nonconstant shear: a model of midlatitude squall lines. *Q. J. Roy. Meteor. Soc.*, **108,** 739–762.

Weisman, M. L., J. B. Klemp and R. Rotunno, 1988: Structure and evolution of numerically simulated squall lines. *J. Atmos. Sci.*, **45,** 1990–2013.

Zhang, D.-L., 1989: The effect of parameterized ice microphysics on the simulation of vortex circulation with a mesoscale hydrostatic model. *Tellus,* **41A,** 132–147.

——, and J. M. Fritsch, 1986: Numerical simulation of the mesoβ scale structure and evolution of the 1977 Johnstown flood. Part I: Model description and verification. *J. Atmos. Sci.*, **43,** 1913–1943.

——, and ——, 1988a: Numerical sensitivity experiments of varying model physics on the structure, evolution and dynamics of two mesoscale convective systems. *J. Atmos. Sci.*, **45,** 261–293.

——, and ——, 1988b: A numerical investigation of a convectively generated, inertially stable, extratropical warm-core mesovortex over land. Part I: Structure and evolution. *Mon. Wea. Rev.*, **116,** 2660–2687.

——, E.-Y. Hsie and M. W. Moncrieff, 1988: A comparison of explicit and implicit predictions of convective and stratiform precipitating weather systems with a mesoβ-scale numerical model. *Q. J. Roy. Meteor. Soc.*, **114,** 31–60.

——, K. Gao and D. B. Parsons, 1989: Numerical simulation of an intense squall line during 10–11 1985 PRE-STORM. Part I: Model verification. *Mon. Wea. Rev.*, **117,** in press.

Zipser, E. J., 1969: The role of organized unsaturated downdrafts in the structure and rapid decay of an equatorial disturbance. *J. Appl. Meteor.*, **8,** 799–814.

——, 1977: Mesoscale and convective-scale downdrafts as distinct components of squall-line circulation. *Mon. Wea. Rev.*, **105,** 1568–1589.